CHALMERS
UNIVERSITY OF TECHNOLOGY

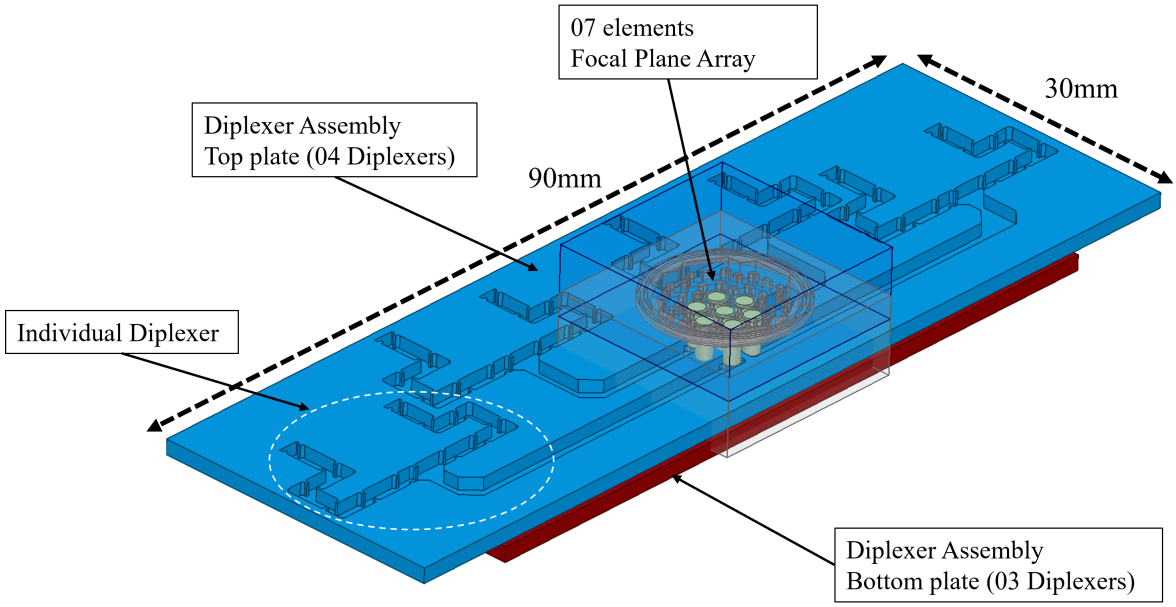

Steerable Extreme High Gain Antenna System for 5 and 6G Wireless Transport

Master's thesis in Antenna Systems Research Group Chalmers and Ericsson Research

SOHAIB YAQOOB CHAUDHRY

DEPARTMENT OF Electrical Engineering
CHALMERS UNIVERSITY OF TECHNOLOGY
Gothenburg, Sweden 2023
www.chalmers.se

Master's thesis 2023

Design of a compact W-Band Diplexer Assembly for Integration with Focal Plane Array fed Reflectors

Master's thesis in Antenna Systems Research Group Chalmers and Ericsson Research

SOHAIB YAQOOB CHAUDHRY

CHALMERS
UNIVERSITY OF TECHNOLOGY

Department of Electrical Engineering
Communications, Antennas, and Optical Networks Division
Antenna Systems Research Group
Chalmers University of Technology
Gothenburg, Sweden 2023

Design of a compact W-Band Diplexer Assembly for
Integration with Focal Plane Array fed Reflectors
SOHAIB YAQOOB CHAUDHRY

Supervisor: Artem Vilenskiy, Viktor Chernikov, Antenna Systems Research Group
Chalmers || Sam Agneessens, Lars Manholm, Ericsson Research Gothenburg
Examiner: Prof. Marianna Ivashina, Antenna System Research Group Chalmers

Master's Thesis 2023
Department of Electrical Engineering
Communications, Antennas, and Optical Networks
Antenna Systems Research Group
Chalmers University of Technology
SE-412 96 Gothenburg
Telephone +46 31 772 1000

Cover: 07-Diplexers integrated with a W-band Focal Plane Array

Typeset in LaTeX
Printed by Chalmers Reproservice
Gothenburg, Sweden 2023

Design of a compact W-Band Diplexer Assembly for
Integration with Focal Plane Array fed Reflectors
Sohaib Yaqoob Chaudhry
Department of Electrical Engineering
Chalmers University of Technology

Abstract

The rapid advancement of 5G and 6G technologies has ushered in a new era of wireless communication, demanding higher performance capabilities. To meet these demands, Radio Access Networks (RANs) are increasingly utilizing higher frequencies to enhance channel capacity. Wireless backhaul networks are also exploring the potential of operating at even higher frequencies, such as the W-band (92GHz-114GHz), to enable high-capacity networks. Recent trials have demonstrated that W-band performs on par with E-band and offers a wider untapped spectrum for high-capacity wireless transport. However, the deployment of high-gain antennas necessary for long-distance, high-capacity, and robust W-band links poses challenges in terms of tower stability requirements. To address these challenges, the Vinnova-funded Project at the Chalmers University of Technology is focused on a novel solution—an electronically steerable antenna system with high-gain capabilities operating in a Frequency Division Duplex (FDD) configuration for backhaul links. The research objective is to enable FDD configuration in electronically steerable antennas through the design and integration of a compact W-band Diplexer Assembly.

The primary objective of this master's thesis is to design and optimize a compact W-band diplexer utilizing the K-Impedance Inverter and Coupling Matrix Method. The design comprises ten iris-coupled resonator cavities assembled with a power divider in a T-junction topology. The resulting diplexer exhibits a 5^{th} order Chebyshev type frequency response centered at 95.5GHz and 107.5GHz, respectively, with each diplexer channel providing an effective bandwidth of 3GHz. The diplexer achieves a maximum passband return loss of -15dB and an insertion loss of less than 1 dB. The design underwent multiple optimization strategies to reduce overall volume while maintaining high manufacturing tolerances of $\pm$15um. These strategies included symmetrical and asymmetrical inductive and capacitive iris-based filters, dual-mode and higher-order-mode cavity resonators (TE_{10n}), H-plane T-junction, and the evanescent mode filters. The use of higher-order (TE_{102}) mode filters proved to be the optimal strategy, resulting in a compact diplexer assembly manufactured using precision CNC milling. The performance of the diplexer assembly was validated through laboratory measurements. A comprehensive competitive analysis was conducted, comparing the implemented design technique with available designs in the literature to evaluate advantages and drawbacks. Finally, the diplexer assembly was seamlessly integrated with the available Focal Plane Array, and a 3D Electromagnetic (EM) Model was generated to complete the research objectives.

Keywords: W-Band, Steerable Antennas, Waveguide, Filters, Higher-order modes, Diplexer, FDD, 5G and 6G, Wireless Transport.

Acknowledgements

I am deeply indebted to Prof. Marianna Ivashina, my esteemed examiner, for providing me with the invaluable opportunity to embark on this captivating research journey. Her unwavering encouragement and support have played a pivotal role in the successful completion of my research. Prof. Marianna's outstanding expertise and unwavering dedication to research have been a constant source of inspiration, propelling me to strive for excellence in all my endeavors. I would like to express my sincere gratitude to Prof. Marianna and her team for their engaging discussions and invaluable feedback throughout my research work with the Antenna Systems Research group since June 2022. Their patience, guidance, and unwavering support have significantly contributed to both my personal and academic growth. I am truly grateful for the enriching experiences and knowledge gained through our collaborations. I extend my heartfelt gratitude to my supervisors, Viktor Chernikov and Artem Vilenskiy, for their invaluable guidance and mentorship throughout this research endeavor. Viktor Chernikov has been an exceptional mentor, demonstrating unwavering dedication, diligence, and boundless energy. His exemplary work ethic serves as an inspiration to all members of the department. I am truly grateful for his support and the valuable insights he has provided, which have significantly contributed to the success of this study. I would also like to extend my appreciation to Artem Vilenskiy for his guidance and support, which have been instrumental in shaping the direction and outcomes of this research. His expertise, encouragement, and scholarly guidance have played a vital role in my academic and personal growth, and I am honored to have had the opportunity to work under his supervision.
I would like to express my profound appreciation to Sam Agneessens and Lars Manholm from Ericsson Research, Gothenburg, Sweden, for their exceptional knowledge and expertise. Their invaluable contributions played a pivotal role in the success of my research endeavor, as their guidance and support greatly influenced the outcomes of my thesis. I am truly grateful for their commitment to excellence, which not only enriched my work but also deepened my understanding of the field. I am obliged to express my sincere gratitude to my colleagues (research thesis opponents) Jamal and Karl for their invaluable contributions and collaborative endeavors throughout the concluding phase of my research thesis. Their insightful discussions and diverse perspectives proved instrumental in elevating the caliber of my work. Furthermore, I am deeply grateful to my parents for their kind support and encouragement throughout my academic journey. Their constant backing has driven my accomplishments, and I am truly indebted to them. Finally, I would like to acknowledge my beloved wife, Abeera, for her patience and understanding during my pursuit of a master's degree. Despite the challenges, we managed to create cherished memories together and her presence has been an immense source of strength and motivation for me. This work has received funding from the "ENERGETIC" Project supported by VINNOVA (2021-01337).

Sohaib Chaudhry, Gothenburg, June 2023

List of Acronyms

Below is the list of acronyms that have been used throughout this thesis listed in alphabetical order:

FDD	Frequency Division Duplex
TDD	Time Divison Duplex
3D	Three Dimensional
BW	Bandwidth
CMM	Coupling Matrix Method
EM	Electromagnetic
FDTD	Finite Difference Time Difference
FEM	Finite Element Method
HFSS	High-Frequency Simulation Software
MoM	Method of Moment
QW	Quarter-wavelength
S-param	Scattering parameters
TE	Transverse Electric
TM	Transverse Magnetic
WG	Waveguide
FPA	Focal Plane Array
BFN	Beamforming network
PC	Power Combiner
COETW	Circular Open-Ended Teflon-filled Waveguide
CNC	Computer Numerical Control
CST	Computer Simulation Technology
WR	Reactangular Waveguide

Nomenclature

Below is the nomenclature of indices, sets, parameters, and variables that have been used throughout this thesis.

Indices

i,j	Indices for number of resonators
$10n$	Resonator cavity higher order modes

Sets

$\mathcal{N}$	No. of poles/ resonators in a filter
$\mathcal{W}$	Opening window / Width of Iris
$\mathcal{L}$	Length of cavity resonators
$\sqcup$	thickness of iris (discontinuity)

Parameters

λ_g	Guided wavelength in rectangular waveguide
X_p, X_s	Equivalent circuit T-junction parameters
Z_0	Characteristic Impedance
Z_L	Load Impedance
$\phi_{i,j}$	Modified equivalent circuit T-junction parameter
$K_{i,j}$	K-Impedance inverter parameters
f_{res}	Resonance frequency of a waveguide cavity
f_{cutoff}	Cutoff frequency of a rectangular waveguide
f_c	Center frequency
f_0	Center frequency

f_e	Even mode resonant frequency
f_m	Odd mode resonant frequency
$k_{i,j}$	Physical coupling elements between cavity resonators
$S_{i,j}$	Scattering parameters of one or more port(s) circuit
Q_e	External quality factor
Q_u	Unloaded quality factor
Q_l	Loaded quality factor
Q_c	Conductor loss of cavity wall
Q_d	Dielectric loss
$M_{i,j}$	Coupling matrix elements
L_{cap}	Length of cavity resonator constituting capacitive aperture
L_{ind}	Length of cavity resonator constituting inductive aperture
c	speed of light
a	Width of waveguide
b	Height of waveguide

Variables

g_n	Chebyshev lumped-elements lowpass prototype elements

Contents

List of Figures

List of Tables

1
Introduction

1.1 Wireless Backhaul Networks

Wireless backhaul networks play a critical role in connecting the Radio Access Network (RAN) to the core network in cellular communication systems. As technology advances, the demands on these networks become more complex. To address these challenges, exploration of the sub-THz frequency range, such as the W-band, is crucial. However, W-band links face various challenges, including high signal attenuation or free space path loss, necessitating the use of high-gain antennas with increased directivity. Unfortunately, high directivity antennas often have narrower beamwidths (typically $\leq 0.5 degrees$), which can pose alignment issues for point-to-point communication links due to mast sway induced by external factors like wind, solar effects, and installation platform limitations.
In response to these challenges, Project ENERGETIC proposes a solution that involves designing and deploying high-gain, electronically steerable antennas utilizing spatial power combination techniques in a Frequency Division Duplex (FDD) configuration. This innovative approach eliminates the need for mechanically steerable antennas, external alignment tools, and rigid masts, providing a more efficient and flexible solution for wireless backhaul networks.

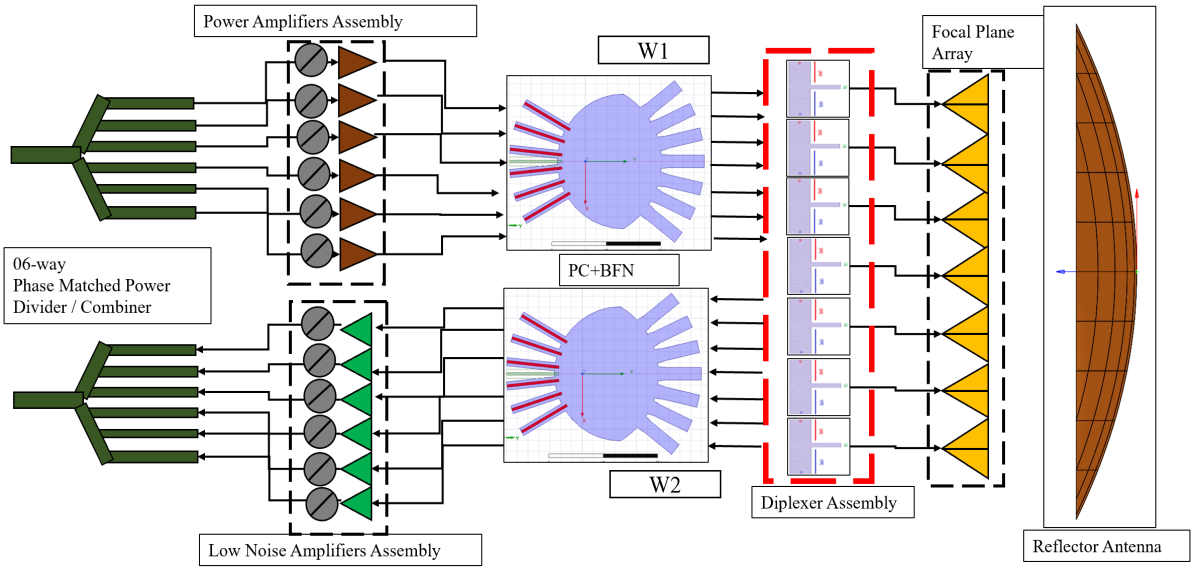

Figure 1.1: Block Level Diagram of Project ENERGETIC

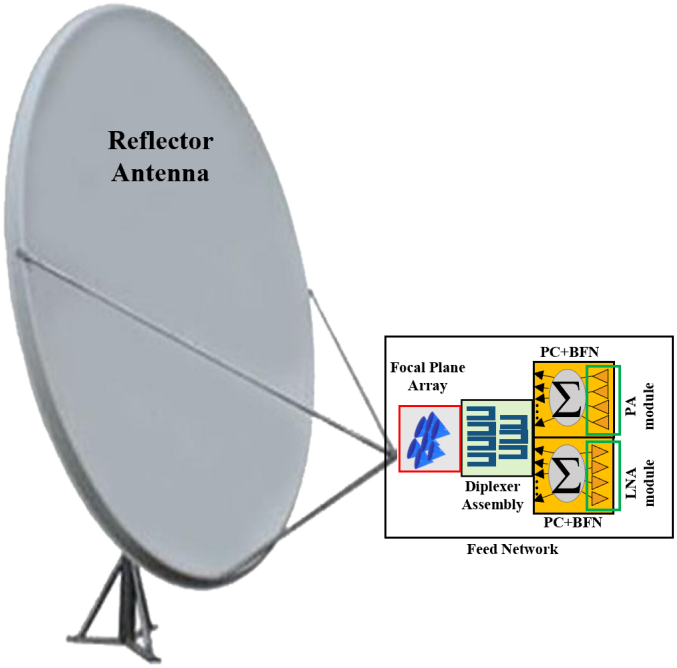

Figure 1.2: Anticipated Antenna Architecture Diagram

The block-level diagram and anticipated antenna architecture illustrate the transmission (TX) and reception (RX) chains of the wireless backhaul antenna system. The TX RF frontend pathway begins with a 1-to-6 power splitter, which is connected to a power amplifier assembly consisting of six distinct power amplifiers and phase shifters. This assembly is then linked to a Rotman lens-shaped parallel plate waveguide module that facilitates spatial power combination and beam-switching capabilities [5]. A focal plane array integrated with a diplexer assembly is used to illuminate the reflector antenna in a star-shaped configuration with seven beams. The diplexer assembly comprises seven individual diplexers and is tightly integrated with the individual elements of the focal plane array, as well as the power combiner and beamforming networks for both the TX and RX chains.

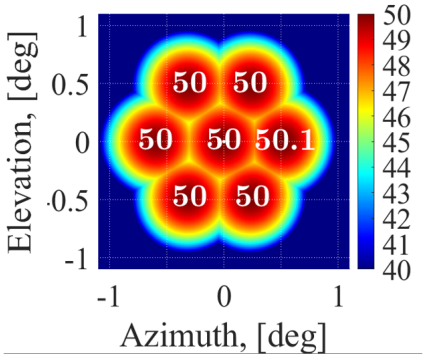

Figure 1.3: FPA Beamshape / Layout

Electronic steering plays a vital role in the proposed solution, allowing for precise and efficient beam steering without the requirement for manual alignment. This approach offers substantial cost savings in terms of development and deployment for wireless backhaul networks, making it an exceptionally cost-effective option. By eliminating the need for manual alignment, the solution streamlines the installation process and reduces ongoing maintenance costs, while still ensuring optimal performance and reliable connectivity.

1.2 Thesis Motivation

The deployment of sub-THz frequency range commercial antennas for wireless backhaul networks necessitates the exploration of advanced antenna technologies. These antennas typically operate in a frequency division duplex (FDD) configuration, supporting multiple sub-bands or frequency bands such as E-band and sub-5G band. In recent years, commercially available mechanically steerable antennas have gained attention but are accompanied by inherent limitations, such as a limited lifespan due to mechanical wear. Consequently, there is a growing demand for the development of electronically steerable antennas to overcome these challenges
In the Vinnova-funded project at Chalmers, a pioneering approach to electronically steerable antennas for point-to-point links has been proposed. This approach leverages spatial power combination techniques to achieve the demanding requirement of high directivity, aiming for at least 50dBi. The specific objective of this research thesis is to realize a fully operational implementation of the proposed steerable antenna system by incorporating a Frequency Division Duplex (FDD) configuration. To comprehensively address this objective, the thesis extensively examines the theoretical and practical aspects associated with FDD and TDD configurations. It also investigates the challenges involved in implementing the FDD configuration in electronically steerable antennas. These challenges include efficient frequency filtering, compact Diplexer assembly, and seamless integration into the antenna system.
The overarching goal of this research work is to contribute to the advancement of next-generation wireless backhaul networks by providing a comprehensive understanding of the capabilities and limitations of electronically steerable antennas in an FDD configuration. By addressing the research question and exploring the associated challenges and benefits, this thesis aims to offer valuable insights for the development of future wireless backhaul networks.

1.3 Frequency Channel Planning

The determination of the operational frequency band is a critical undertaking during the planning phase, particularly concerning the development of bandpass filters. Within Project ENERGETIC, our objective is to focus on two specific sub-bands that have a separation of approximately 12GHz (center to center). The comprehensive frequency arrangement for the W-band, with emphasis on the designated sub-bands for this research study, is visually depicted in the accompanying figure below:

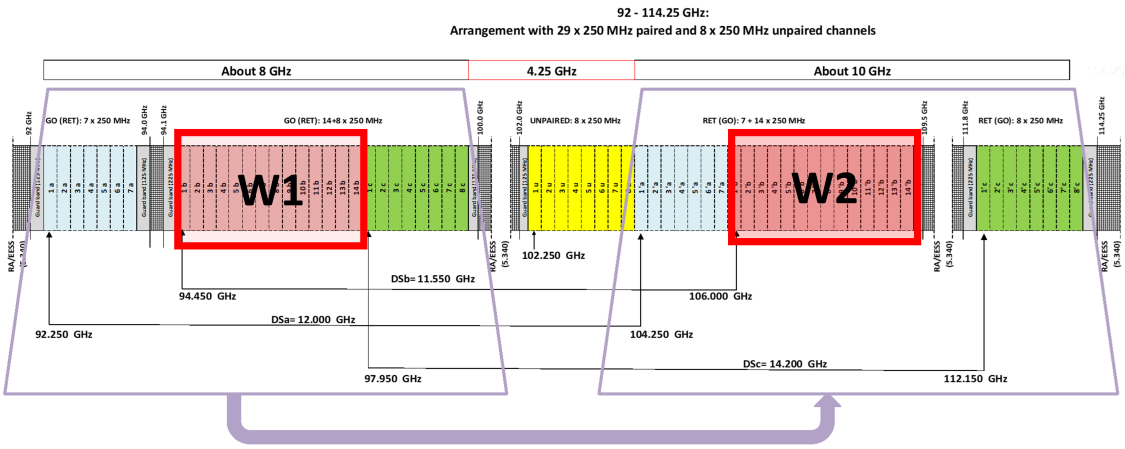

Figure 1.4: W-band Channel Plan [1]

1.4 Specifications

The table below presents the comprehensive specifications for the Diplexer assembly:

Table 1.1: Diplexer Specifications

Parameters	Specifications
Bandpass filter channel 1	94-97 GHz
Bandpass filter channel 2	106-109 GHz
Return loss	$\leq$-15dB
Insertion loss	<-1dB
Isolation between output channels	better than 40dB

1.5 Goals and Tasks of Thesis

The objectives of this research thesis work are outlined as follows:

- Development of an electromagnetic (EM) model and mechanical design for waveguide-based bandpass filters capable of covering the W1 and W2 sub-bands.
- Design of a common input T-junction to facilitate the duplexing of both bandpass filters, resulting in a compact diplexer assembly.
- Formulate an appropriate solution by conducting an extensive sensitivity analysis and implementing a compactness strategy specifically tailored for the diplexer assembly.

- Preparation of a mechanical design for an experimental diplexer assembly prototype, including considerations for manufacturing processes and performance validation through laboratory measurements.
- Design of a mechanical model to facilitate the seamless integration of the Diplexer Assembly with the existing Focal Plane Array (FPA) designs.

1.5.1 Design Tasks

Research and Literature Review A comprehensive literature review is conducted to identify existing bandpass filters and diplexer assemblies with compact layouts. Special attention is given to their dimensional sensitivity, effectiveness, and fundamental limitations.
Analytical and Theoretical Modelling Various design architectures are analyzed and evaluated through analytical and theoretical models. Multiple approaches are considered and refined to achieve the desired outcome.
Numerical simulations The finalized architectures are implemented in designated software packages for individual bandpass filters and diplexer assemblies. Extensive numerical simulations are performed to assess their performance and characteristics.
Design optimization for performance specifications and manufacturability Design optimization is carried out using well-established methods to closely approach the desired specifications. Practical constraints and manufacturability considerations are taken into account during the optimization process..
Design Manufacturing and Performance Validation The optimized design is prepared for manufacturing using standard WR-10 waveguide dimensions with UG-387/U-M flanges. The mechanical design is fabricated through precision CNC milling. Performance validation is conducted through laboratory measurements to ensure the design meets the desired specifications.
Thesis Defense and Project Report Writing The design methodologies, testing procedures, results, conclusions, and future recommendations are presented and discussed in the thesis defense. A comprehensive project report is prepared to summarize the research findings and insights.
Overall, this research thesis report covers a range of design tasks and methodologies, from literature review and theoretical modeling to numerical simulations, design optimization, manufacturing, and performance validation. The findings and conclusions contribute to the advancement of bandpass filters and diplexer assemblies in terms of performance, manufacturability, and practical applications.

1.6 Introduction to Diplexers

"In point-to-point communication links, the accurate management and separation of diverse signals are imperative. A fundamental component in these systems is the diplexer, which fulfills the essential task of filtering and directing multiple frequency channels or bands to their respective output ports within a common transmission line. Additionally, diplexers possess the capability to merge signals of varying frequencies from separate input channels into a singular output port. In the context of terrestrial communication systems utilizing point-to-point radios at the W-band,

microwave diplexers, and multiplexers assume critical roles. These components effectively handle and organize multiple signals, ensuring their optimal transmission with minimal RF interference.
Diplexers are typically engineered using circular or rectangular waveguides, printed circuit boards, or ceramic structures. They integrate bandpass filters with narrow bandwidths and sharp roll-off rates, effectively combined through a diplexing junction. This junction assumes paramount importance in diplexer designs, particularly in waveguide architectures. Its primary function is to facilitate the transmission of the desired RF signals while effectively rejecting any undesired or out-of-band RF signals. To achieve low reflection coefficients at both desired frequency bands, impedance-matching elements are commonly employed within this region. In our present application, we focus on the design of a diplexer assembly employing a rectangular waveguide.

1.6.1 Technologies employed in diplexers design

There are various state-of-the-art technologies utilized in the design of diplexers, which enable the efficient management of multiple signals and the transmission of desired signals with minimal interference. Some of these technologies include:
Planar technologies, such as microstrip and coplanar waveguide (CPW) structures, which offer low profile and compact size designs suitable for high-density and low-frequency applications.
Substrate Integrated waveguide, which allows for high power handling capabilities and excellent isolation between channels.
Microwave monolithic integrated circuit (MMIC) technology which provides high levels of integration and compatibility with microwave systems.
Resonator-based designs, which can offer steep rejection slopes and narrow bandwidths.
Ceramic-based designs, which offer good temperature stability and high Q-factor.
Surface acoustic wave (SAW) technology, which can provide high selectivity and low insertion loss.
When it comes to diplexer design, there are numerous technology options available. The specific diplexer technology selected depends on various application requirements, including but not limited to frequency range, bandwidth, power handling, and size constraints.

1.7 Filter Theory

The initial step in diplexer implementation involves the design of bandpass filters tailored to specific requirements. A filter serves as a frequency selective device with two ports, aiming to attenuate signals within the undesired frequency range (known as the stop-band) while allowing the desired signals (pass-band) to pass through [6], [7]. Filters can be classified in various ways, including attenuation characteristics such as low-pass, high-pass, band-pass, and band-stop. Additionally, filters can be categorized based on different response functions, including Chebyshev, Butterworth, Equiripple, and Elliptical filters [8]. Filter theory forms the foundation

for understanding and designing microwave filters. It provides the principles and mathematical models used to analyze and synthesize filters with desired frequency responses. Microwave filters are designed to selectively pass or reject specific frequency ranges according to the application requirements.

1.8 Microwave Filters Design

Microwave filters can be designed using different methods, each suited for specific applications and frequency ranges. The three main design methods for microwave filters are lumped element, distributed element, and waveguide filters.

1.8.1 Lumped Elements Filters

Lumped elements are passive components that are reciprocal in nature, such as resistors, capacitors, and inductors. A lumped element RF filter is a passive device whose size across any dimension is much smaller than the operating wavelength, resulting in minimal change in the phase of a waveform between input and output ports. Thus, lumped element filters are characterized by lower cost, smaller footprint, and wide bandwidth characteristics. They are primarily used for lower frequencies and possess high power handling capacity. However, the implementation of lumped elements becomes challenging at higher frequencies

1.8.2 Distributed Elements Filters

A distributed elements filter is a type of electronic filter where capacitance, inductance, and resistance are not localized in discrete components but rather integrated within the transmission lines. These distributed elements are commonly utilized at higher frequencies, particularly in the microwave frequency band. Additionally, waveguide cavity resonators can also be regarded as distributed elements in microwave filters.

1.8.3 Waveguide filters

These are electronic devices that are designed to allow specific frequencies to pass through while blocking others. There are several methods for designing waveguide filters, including

Cavity resonator method This method involves designing a cavity resonator with a certain resonant frequency that matches the desired frequency for the filter. The cavity resonator is then coupled with the waveguide to create the filter [9].

Irises method This method involves inserting irises, which are small metal plates, into the waveguide at specific distances. These irises create resonances in the waveguide structure, that serves as building blocks for the filters. [10].

Combline method This method involves using a series of resonant cavities that are coupled together. The coupling between the cavities determines the frequency response of the filter[9].

Interdigital method This method involves using a series of interdigitated fingers

in the waveguide. The fingers act as a bandpass filter, allowing only certain frequencies to pass through[2].
Stepped impedance method This method involves creating a series of stepped impedance sections in the waveguide. The stepped impedance sections act as lowpass or highpass filters, depending on the design [7].

1.9 Filter Simulation Techniques

There are multiple simulation techniques used for designing and optimizing microwave filters including:
Finite Element Method (FEM): This technique divides the filter structure into interconnected elements, solving Maxwell's equations for each element to analyze field distributions, resonant frequencies, and scattering parameters [11]. In this thesis, we utilized the EM Simulator (HFSS), which is based on the Finite Element Method (FEM) principles.
Finite Difference Time Domain (FDTD): In this method, Maxwell's equations are discretized on a grid, then updating the electromagnetic fields in time steps to simulate wave propagation, transient and steady-state responses, and analyze filter characteristics [12].
Method of Moments (MoM): This process solves integral equations derived from Maxwell's equations by representing the filter structure with unknown currents or charges on its surfaces, providing insights into impedance matching, insertion loss, and return loss, particularly for planar structures and antenna arrays [13].

1.10 Performance Characterization

Microwave filters are evaluated based on several performance metrics, including bandwidth, Q-factor, selectivity, and group delay. These performance metrics are critical for evaluating the effectiveness and suitability of microwave filters for specific applications. Designers aim to optimize these metrics based on the specific requirements of the system to achieve desired performance characteristics.
Bandwidth: Bandwidth refers to the range of frequencies over which a filter operates effectively. It represents the frequency span between the lower and upper cutoff frequencies and determines the range of signals that can pass through the filter with acceptable performance.
Q-factor: The Q-factor, also known as quality factor or figure of merit, quantifies the selectivity of a filter. It is the ratio of the center frequency to the bandwidth and indicates how well the filter can discriminate between desired and undesired frequencies. Higher Q-factors represent narrower bandwidths and higher selectivity.
Selectivity: Selectivity measures a filter's ability to attenuate signals outside its passband. It indicates how effectively a filter can suppress undesired frequencies while allowing desired frequencies to pass through. Higher selectivity corresponds to better out-of-band signal rejection.
Group Delay: Group delay measures the time delay experienced by different fre-

quency components of a signal passing through a filter. It is important in applications where maintaining the phase relationship of signals is crucial, such as in communication systems. Low group delay ensures minimal distortion and phase shifts across the filter's passband.

1.11 Optimizing Waveguide filter Size through Compact Design Strategies

Waveguide filters play a crucial role in microwave engineering, and optimizing their size without compromising performance is a significant challenge. Compact design strategies offer a promising solution by reducing the size and weight of waveguide filters while maintaining their desired performance characteristics. These strategies encompass innovative material usage, component miniaturization, and filter topology optimization, resulting in versatile, cost-effective filters suitable for various applications. This research thesis focuses on the optimization of the waveguide filter size, exploring different methods for size and performance enhancement. A literature review was carried out for specific compact design methodologies and summarized in a subsequent section.

1.11.1 Inductive irises in direct-coupled waveguide filters

Inductive irises are strategically placed within direct-coupled waveguide filters to control coupling and achieve the desired frequency response. By adjusting iris dimensions, spacing, and the number of irises used, the passband, stopband, and attenuation characteristics of the filter can be precisely controlled. For the waveguide filter design, an inductive structure or iris induces a negative length in the resonator [3]. Incorporating inductive irises not only reduces the overall volume and size of the cavities but also maintains the filter's frequency response.

1.11.2 Quarter wavelength Cavity Resonators

Quarter-wavelength cavity resonators, another compact design approach, are resonant structures commonly used in microwave and RF applications. These compact resonators, designed to resonate at specific frequencies determined by their dimensions, are widely used in filter designs. By combining multiple resonators, bandpass or band-stop filters can be created, offering advantages such as compact size, high quality factor (Q-factor), and excellent frequency selectivity. They find applications in wireless communication systems and radar systems that require narrowband filtering. [14].

1.11.3 Evanescent mode filters

Evanescent mode filters, which utilize evanescent wave coupling between resonators to achieve frequency selectivity, are also explored. These filters rely on the concept of evanescent modes, where electromagnetic waves decay exponentially within

waveguides or resonators [2]. Evanescent mode filters, commonly implemented in waveguide or microstrip technologies, are renowned for their compact size, high selectivity, and low insertion loss. They find applications in wireless communication systems, radar systems, and satellite communication systems.
By investigating these compact design strategies, this research contributes to the advancement of waveguide filters, offering insights into size optimization techniques while maintaining performance requirements. The findings have implications for diverse microwave engineering applications, enabling the development of more efficient and compact filter designs.

2

Design and Realization of Filters

The methodology adopted in this research work encompasses the individual design of filters for the W1 and W2 sub-bands, as well as the independent design of the T-junction. Subsequently, these three modules are integrated to form a compact diplexer assembly. This chapter provides a comprehensive overview of the design techniques employed, the conducted analysis, and the performance evaluation of the waveguide filters.

2.1 Direct-coupled Cavity Resonator Filters

Direct-coupled cavity resonators are a specific type of resonant circuit that consists of multiple resonant cavities directly coupled to each other through shunt inductive apertures and/or series capacitive irises or circular aperture elements. These resonators exhibit desirable characteristics such as a high Q factor, narrow bandwidth, and excellent out-of-band rejection [15]. They find applications in various fields including communication systems, radar systems, and test and measurement equipment.

Direct-coupled cavity resonator filters can be fabricated using two primary methods. The first method involves constructing waveguide cavities with inductive irises, spaced approximately half a wavelength apart, and coupling these individual cavities using quarter-wavelength waveguide transformers. The second method involves directly coupling adjacent cavities using single irises [15]. In this research thesis, the design focuses on direct-coupled resonator filters due to their advantages, including reduced volume, fewer cavities and components, and the ability to operate over wider bandwidths. Recent advancements in iris design procedures have addressed the drawbacks associated with direct-coupled-cavity filters, establishing them as the preferred choice for future applications [15].

To achieve narrow bandwidth in bandpass filters, it is crucial to employ high-Q resonators that are loosely coupled in a cascaded configuration [15] [10]. This study utilizes waveguide structures with shunt inductive irises and half-wave cavity resonators. The waveguide cavity resonators are cross-coupled through apertures in the narrow wall shared by adjacent cavities, with the apertures controlled by shunt inductive irises, as depicted in Figure 2.12.

The conventional approach for designing a half-wave direct-coupled waveguide cavity resonator filter involves utilizing a Chebyshev lowpass prototype as discussed in section 2.1.1. By leveraging the relationship between shunt inductive irises and impedance inverters, as introduced by Cohn in [15], it is possible to derive the equiv-

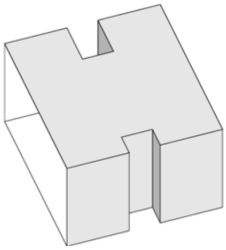

Figure 2.1: Geometry of a Waveguide Cavity resonators, cross-coupled by shunt inductive iris

alent circuit for the filter. This circuit can then be equated to the lowpass prototype linear phase filter [16] at the center frequency. The transformation from the lowpass prototype to the desired bandpass filter is accomplished by replacing the components of the lowpass filter circuit with shunt susceptances and series reactances, represented by LC circuits [15]

2.1.1 Chebyshev Low-pass Prototype

Bandpass filter synthesis commonly employs the conventional approach of starting from a lowpass (LP) prototype design. The design process involves computing the elements of the lowpass prototype filter for a normalized function, assuming a cut-off frequency of 1 rad/sec and source and load impedances of 1 Ω. Subsequently, the low-pass prototype can be transformed into a highpass, bandpass, or bandstop filter using denormalization equations [17]. This transformation involves scaling the cutoff frequencies and applying appropriate impedance transformations to achieve the desired filter response.

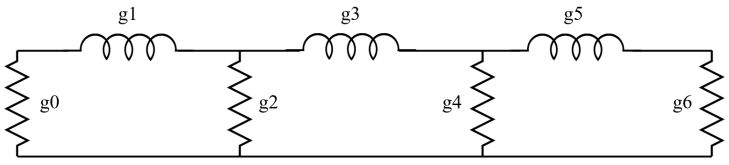

Figure 2.2: Lowpass filter prototype, N=5

Equation 2.1 provides analytical expressions to compute the values of LP prototype elements g_0, g_1 ....., g_{N+1}, where N represents the filter order. Nonetheless, textbooks like [2, 8, 10] offer tabulated values of these elements with different passband ripples. For instance, Table 2.1 lists the element values of Chebyshev LP-prototype filters with a passband ripple of 0.01dB.

$$
\begin{aligned}
g_0 &= 1 \\
\beta &= ln(coth(\frac{L_{AR}}{17.37})) \\
\gamma &= sinh(\frac{\beta}{2n}) \\
a_k &= sin[\frac{(2k-1)\pi}{2n}], \quad k = 1, 2, ..., n \\
b_k &= \gamma^2 + sin^2(\frac{k\pi}{n}), \quad k = 1, 2, ..., n \\
g_1 &= \frac{2a_1}{\gamma} \\
g_k &= \frac{4a_{k-1}a_k}{b_{k-1}g_{k-1}} \\
g_{n+1} &= \begin{cases} 1 & \text{if } n \quad odd \\ coth^2(\frac{\beta}{4}), & \text{if } n \quad even \end{cases} \\
g_{n+1} &= 1
\end{aligned}
\tag{2.1}
$$

Table 2.1: Element values for Nth order Chebyshev LP prototype filter with normalized input impedance $g_0 = 1$, cutoff frequency $\omega_c = 1$Hz and passband ripple $L_{\mathrm{AR}} = 0.01$dB [9]

N	g_1	g_2	g_3	g_4	g_5	g_6	g_7	g_8	g_9	g_{10}
1	0.0960	1.0000								
2	0.4488	0.4077	1.1007							
3	0.6291	0.9702	0.6291	1.0000						
4	0.7128	1.2003	1.3212	0.6476	1.1007					
5	0.7563	1.3049	1.5773	1.3049	0.7563	1.0000				
6	0.7813	1.3600	1.6896	1.5350	1.4970	0.7098	1.1007			
7	0.7969	1.3924	1.7481	1.6331	1.7481	1.3924	0.7969	1.0000		
8	0.8072	1.4130	1.7824	1.6833	1.8529	1.6193	1.5554	0.7333	1.1007	
9	0.8144	1.4270	1.8043	1.7125	1.9057	1.7125	1.8043	1.4270	0.8144	1.0000

2.1.2 Lowpass Prototype to Bandpass Transformation

The process of filter design begins with the crucial step of designing a lowpass filter prototype, which serves as the foundation for creating filters with different characteristics. This design procedure involves three key transformations: Frequency Scaling, Impedance Transformation/Scaling, and Filter Type Scaling.
In Frequency Scaling, the cutoff frequency of the lowpass filter prototype is normalized to 1 rad/s. To reference another frequency, the values of the filter elements need to be adjusted so that they maintain the same impedance at the scaled frequency. The specific method of frequency transformation varies depending on the desired filter type.
Impedance Transformation/Scaling is another important aspect of the design process. It involves adjusting the impedance levels of the filter prototype to match

the desired impedance values for a specific application. This transformation ensures optimal performance and compatibility with the target system.
Filter Type Scaling pertains to transforming the lowpass filter prototype into different filter types, such as bandpass or bandstop filters. For instance, in the case of a bandpass filter, the lowpass filter response is considered for both positive and negative frequencies, as depicted in Figure 2.3a. This response is then shifted in frequency to obtain the desired bandpass response illustrated in Figure 2.3b. The transformation ensures the filter meets the required frequency specifications and achieves the desired filtering characteristics.

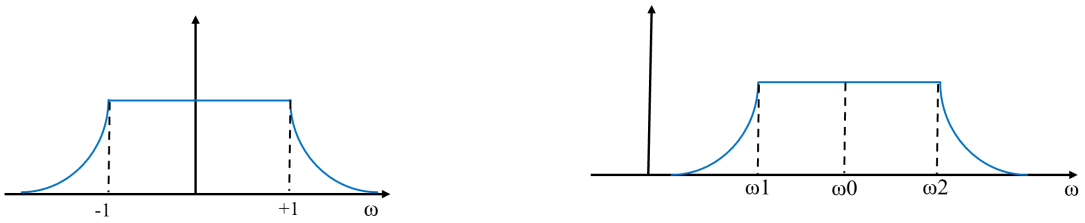

(a) **(b)**

Figure 2.3: Frequency responses in lowpass to bandpass transformation

$$\omega \rightarrow \omega' = \frac{1}{\Delta}[\frac{\omega}{\omega_0} - \frac{\omega_0}{\omega}] \tag{2.2}$$
$$\Delta = \frac{\omega_2 - \omega_1}{\omega_0}$$

Where ω_1 and ω_2 are angular frequencies of the lower and higher passband edges, Δ is the desired bandwidth, and the center frequency ω_0, is defined as the geometric mean $\sqrt{\omega_1\omega_2}$.

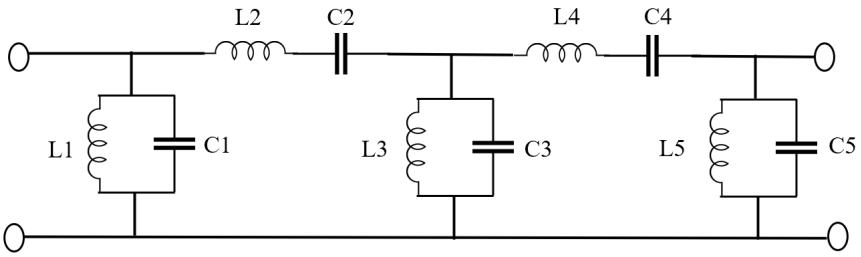

Figure 2.4: Bandpass filter prototype, N=5

2.2 Waveguide Filters Design

This research thesis focuses on two well-established methods for designing direct-coupled cavity resonator filters: the K-impedance inverter method and the Coupling

matrix method. These methods are applicable to various types of coupled resonators, irrespective of their physical structure [1]. The objective of this thesis is to realize the K-impedance inverter and coupling matrix concepts using a rectangular waveguide structure.
The design process for coupled-resonator filters based on rectangular waveguides typically involves the following steps:

- **Specifications Finalization:** Defining the desired filter specifications and determining the filter order based on those specifications.
- **Synthesis:** Synthesizing a K-impedance inverter circuit model or coupling matrix elements that meet the required filter response specifications.
- **Physical Dimensions Extraction:** Extracting the physical dimensions of each waveguide filter component, such as the cavity resonator length and coupling irises widths, using a combination of analytical modeling and electromagnetic (EM) simulation techniques.
- **Filter 3D model Design:** Designing the complete filter using an EM simulator, utilizing the previously extracted physical dimensions. The design is optimized to meet the desired specifications.
- **Sensitivity Analysis:** Performing sensitivity analysis on the entire structure to identify potential tolerances related to manufacturing errors. This step helps assess the robustness of the design and identify critical parameters.
- **Manufacturing and Evaluation:** Fabricating the filter based on the design specifications and assessing its performance using a Vector Network Analyzer (VNA). If the measured response significantly deviates from the simulated results, additional tuning and optimization may be required to improve the measured performance.

This research thesis focuses on the design, manufacturing, and measurement of direct-coupled cavity resonator filters for W-band. Subsequent sections provide detailed information on the specific methodologies employed and their outcomes.

2.2.1 Rectangular Waveguide

Waveguides are conducting structures designed to guide and propagate electromagnetic waves along specific paths. They are widely employed in electronic systems, particularly at high frequencies where the wave nature of alternating electromagnetic fields becomes significant. Waveguides can be constructed as a single continuous piece of conducting material or as multiple conductors joined together. The type of waveguide determines the types of waves that can propagate within them, and they may contain either empty space or a dielectric medium. The dimensions and composition of the conductors within the waveguide determine the modes of wave propagation supported. Transverse Electric (TE), Transverse Magnetic (TM), and Transverse Electromagnetic (TEM) are the primary modes of wave propagation supported by waveguides. TEM waves are associated with transmission lines and waveguides composed of more than one conductor, such as parallel plate waveguides. On the other hand, rectangular waveguides, which consist of a single conductor, permit the propagation of TE and TM waves exclusively [8]. These waveguides play a crucial role in guiding and controlling electromagnetic energy in various applications

within the microwave and RF domains.

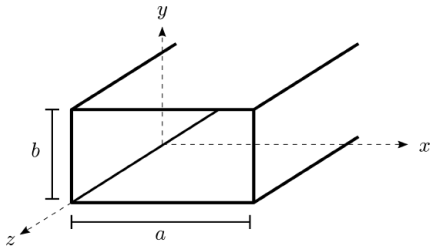

Figure 2.5: Geometry of a rectangular waveguide

The rectangular waveguide, as shown in Figure 2.5, is a hollow metallic pipe guiding electromagnetic waves. By varying the shape of the rectangular waveguide, it can work as a cavity resonator or as a coupling iris to construct the filtering circuit. The cutoff frequency is the lowest frequency that a mode can propagate through the rectangular waveguide. The cut-off frequency of modes is given by the following equation:

$$f_{cutoff} = \frac{c}{2a}\sqrt{(\frac{m\pi}{a})^2 + (\frac{n\pi}{b})^2} \tag{2.3}$$

Where m and n are the number of half-standing waves along the x-axis and y-axis of the rectangular waveguide, and c is the speed of light in a vacuum. The lowest frequency is achieved when m=1 and n=0 if a>b i.e., TE_{10} and is known as the dominant mode of rectangular waveguide.

2.2.2 Resonance Cavities

When a section of a rectangular waveguide is enclosed by additional walls perpendicular to the direction of wave propagation, it creates a cavity structure. This cavity enables the accumulation of electromagnetic energy in the form of standing waves. The presence of these additional walls allows for wave reflection and the possibility of wave propagation in the opposite direction, leading to the formation of standing waves at specific resonance frequencies. The resonance frequencies correspond to the frequencies at which the standing waves within the cavity are most pronounced and can store a significant amount of electromagnetic energy. These resonant modes play a crucial role in the operation of devices such as cavity filters, resonators, and cavity-backed antennas, where the standing waves are exploited to achieve desired functionalities and characteristics.
As shown in Figure 2.6, a cavity resonator is a rectangular waveguide enclosed by a conducting wall at each end. The length of a cavity resonator "d" is multiple of half-guided wavelength $\frac{\lambda_g}{2}$ at the resonant frequency. The resonance frequency of a cavity can be determined similarly to how the cutoff frequency of a waveguide is determined. However, in the case of a cavity, additional boundary conditions are introduced by the conductive walls that close off the ends of the waveguide structure. The resonance frequency of the cavity is given by the following expressions:
In Figure 2.6, a cavity resonator is depicted as a rectangular waveguide with conducting walls at each end. The length of the cavity resonator, denoted as "d" is chosen to be a multiple of half the guided wavelength $\frac{\lambda_g}{2}$ at the resonant frequency.

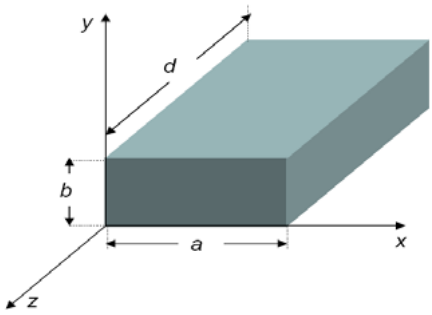

Figure 2.6: Geometry of a rectangular waveguide cavity resonator

The determination of the resonance frequency of a cavity resonator is similar to that of the cutoff frequency in a waveguide. However, the presence of conductive walls at the ends of the waveguide introduces additional boundary conditions. These boundary conditions affect the resonance frequency of the cavity, and it can be expressed using the following equation:

$$f_{res} = \frac{c}{2a}\sqrt{(\frac{m\pi}{a})^2 + (\frac{n\pi}{b})^2 + (\frac{l\pi}{d})^2} \tag{2.4}$$

Where m and n are the number of half-standing waves along the x-axis and y-axis of the rectangular waveguide, c is the speed of light in vacuum, and l corresponds to the resonator cavity mode index. The dominant mode, corresponding to the lowest order resonance frequency of the cavity, is then the TE_{101} mode and for this mode, the guided wavelength λ_g is given by Equation 2.5.

$$\lambda_g = \frac{2ac}{\sqrt{4a^2f^2 - c}} \tag{2.5}$$

Where f is the mode frequency, a is the width of the rectangular waveguide, c is the speed of light in vacuum.

2.2.3 Coupling Irises

A coupling iris is a type of interface between two waveguides that are utilized for coupling purposes. It is a discontinuity that allows for the transfer of energy and signals between the two waveguide resonators.

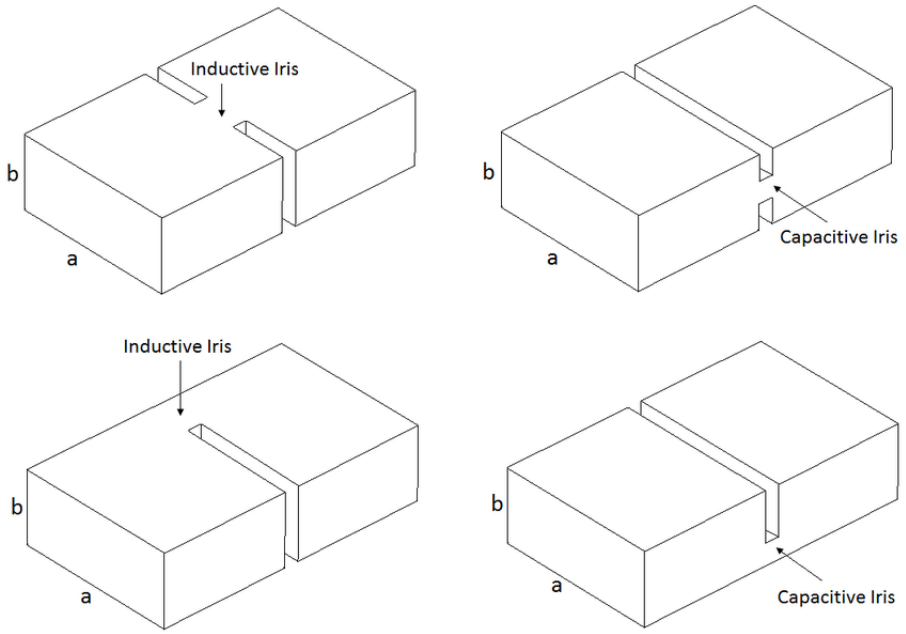

Figure 2.7: Geometry of a rectangular waveguide iris

Standard irises utilized in rectangular waveguide structures are illustrated in Figure 2.7. The iris with vertical slots are the inductive irises i.e., symmetrical and asymmetrical respectively. The iris with horizontal slots are the capacitive irises i.e., symmetrical and asymmetrical respectively.

2.3 Filter design: K-Impedance Inverter Model

The K-impedance inverter model is a widely used technique in microwave filter design. It is based on the concept of a circuit that can invert the impedance of a given network at a specific frequency. The model consists of a transmission line with a characteristic impedance of Z_0 connected in parallel with a shunt impedance Z_L, which can take the form of a resistor, inductor, or capacitor. The K parameter represents the ratio of the shunt impedance Z_L to the characteristic impedance Z_0 [8].

The K-impedance inverter model enables the design of various types of filters, including low-pass, high-pass, band-pass, and band-stop filters. By cascading multiple K-impedance inverter circuits, more complex filter responses can be achieved [18]. This technique offers a simple and effective approach to realize a wide range of filter topologies with low insertion loss and high attenuation [18]. This model has been extensively used in the design of microwave filters for diverse applications such as satellite communications, wireless networks, and radar systems [2].

In this study, Chebyshev filters are employed as examples to demonstrate the utilization of filter circuit models and an electromagnetic (EM) simulator (HFSS) for synthesizing the physical dimensions of the filter. This approach can be extended to other filter functions as well. Figure 2.8 illustrates the K-impedance circuit model for Chebyshev filters.

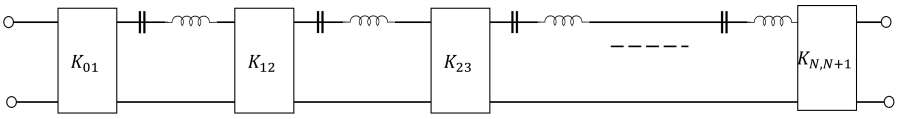

Figure 2.8: Impedance inverter model for Chebyshev filters, [2]

K-Impedance inverter elements $K_{j,j+1}$, are related to the chebyshev lowpass prototype elements g_0, g_1, g_2,..., g_{N+1} as follows [2]:

$$\frac{K_{j,j+1}}{Z_0} = \frac{\pi\Delta}{2\sqrt{g_j g_{j+1}}} \quad j = 1, 2, ..., N-1 \tag{2.6}$$

$$\frac{K_{01}}{Z_0} = \sqrt{\frac{\pi\Delta}{2g_0 g_1}} \quad \frac{K_{N,N+1}}{Z_0} = \sqrt{\frac{\pi\Delta}{2g_N g_{N+1}}} \tag{2.7}$$

$$\Delta = \frac{\lambda_{g1} - \lambda_{g2}}{\lambda_{g0}}$$

The Chebyshev lowpass prototype elements g_0, g_1, g_2, ..., g_{N+1} can be determined based on the desired filter specifications. These elements can be extracted using Equation 2.1 or by referring to Table 2.1, which provides the values corresponding to specific filter requirements.

2.3.1 Design, Optimization, and Analysis of Filter Performance

The block diagram of the five-pole Chebyshev inductive iris-coupled waveguide filter is illustrated in Figure 2.9 and it is formed by two transverse discontinuities separated by waveguide sections.

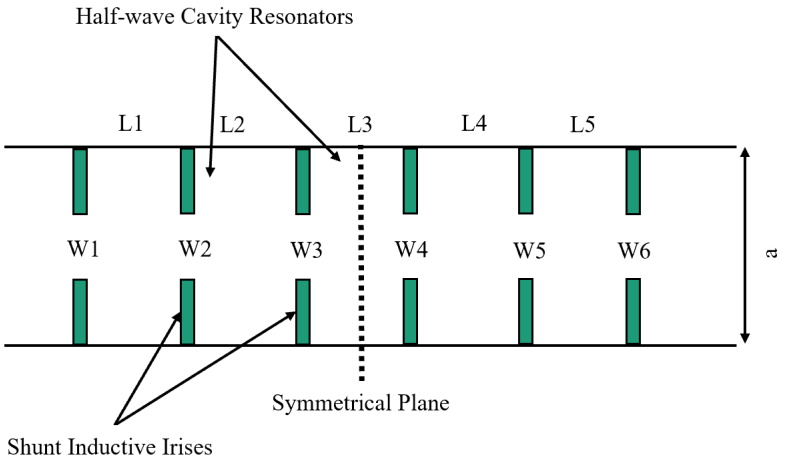

Figure 2.9: Five pole waveguide shunt inductive irises waveguide filter (Top View)

The equivalent circuit of a filter with waveguide irises is shown in Figure 2.10a. In order to adapt the circuit to the K-impedance inverter shape, a section of length $\phi/2$ and $-\phi/2$ is added on each side of the discontinuity, as depicted in Figure 2.10b. This method of adding extra lengths does not alter the original circuit [2], and provides approximate dimensions for the filter. However, optimization of the parameters is necessary to determine the appropriate dimensions that will result in an optimal response for the desired filter [19].

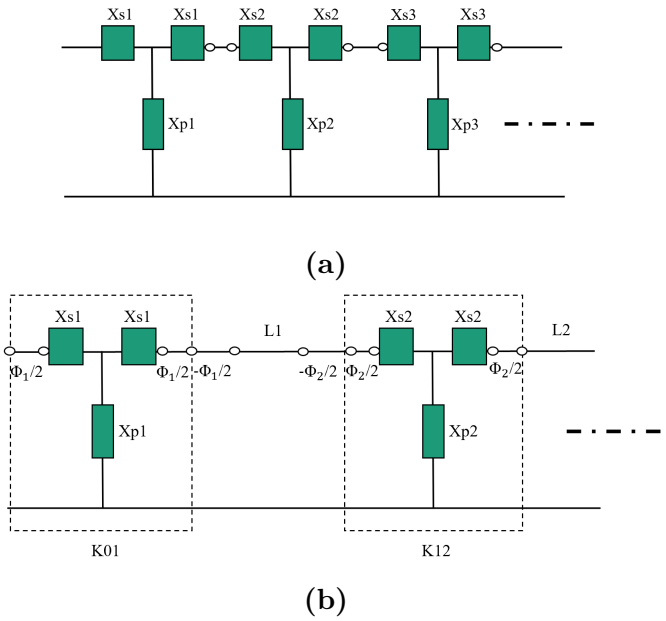

Figure 2.10: Symmetrical Inductive Irises Waveguide filter: (a)Equivalent Circuits and (b)Modified Equivalent ciruit

The scattering matrix *S-parameters* (Figure 2.11a) of the iris (Figure 2.11b) were obtained using an Electromagnetic Simulator (HFSS), and its equivalent network was calculated as illustrated Figure 2.11c. The iris was represented by two series inductors X_s and one parallel inductor X_p.

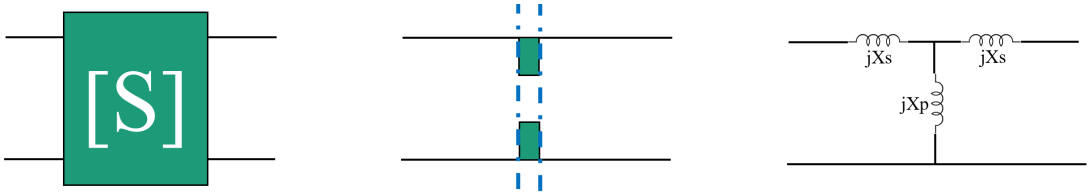

Figure 2.11: Waveguide Iris:(a)S-equivalent (b)Symmetrical Iris (b)Equivalent T-circuit

A unit-cell electromagnetic (EM) simulation, depicted in Figure 2.12, is utilized in this study. The design parameters of the waveguide filter irises are obtained based

on the previously determined values of the K-Impedance inverter elements (2.6, 2.7). These values serve as a basis for determining the specific dimensions and geometry of the irises. The aperture of the iris is systematically varied, and the corresponding S-parameters are computed at the center frequency. Subsequently, the values of X_s, X_p, K, and ϕ are extracted using the mathematical expressions described in [2]. This procedure enables the precise determination of the irises dimensions required for achieving the desired filter performance.

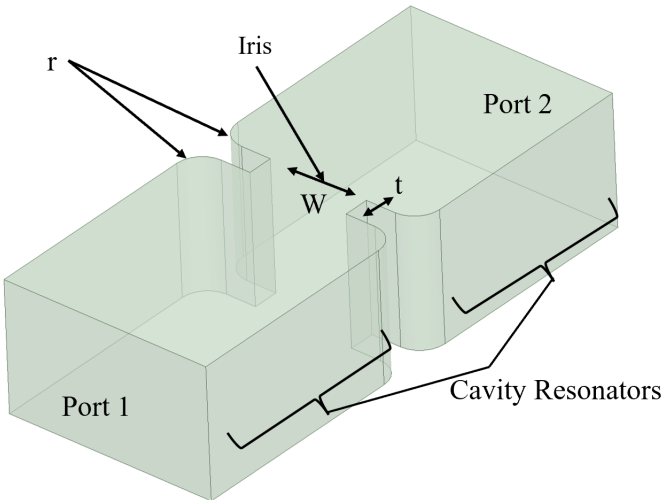

Figure 2.12: 3D-EM model of unit cell used for extraction of K-Impedance Inverter parameters

Equivalent T-network parameters X_s and X_p are computed using mathematical expressions mentioned in Equations 2.8 and 2.9.

$$j\frac{X_s}{Z_0} = \frac{1 - S_{12} - S_{11}}{1 - S_{11} + S_{12}} \tag{2.8}$$

$$j\frac{X_p}{Z_0} = \frac{2S_{12}}{(1 - S_{11})^2 - S_{12}^2} \tag{2.9}$$

Furthermore, K impedance inverter and ϕ values are obtained using T-network parameters through the following expressions:

$$\frac{K}{Z_0} = |\tan(\frac{\phi}{2} + \arctan\frac{X_s}{Z_0})| \tag{2.10}$$

$$\phi = -\arctan(2\frac{X_p}{Z_0} + \frac{X_s}{Z_0}) - \arctan\frac{X_s}{Z_0} \tag{2.11}$$

Thus, knowing the value of K, irises widths (W1-W6; Figure 2.9) are identified and using the corresponding values of ϕ_i, the length of the resonators (L1-L5; Figure 2.9)) are extracted using through the following mathematical expression:

$$l_r = \frac{\lambda}{2\pi}[\pi + \frac{1}{2}(\phi_r + \phi_{r+1})], r = 1, ...N \tag{2.12}$$

In order to facilitate the CNC-milling manufacturing process, a small curvature, referred to as r in Figure 2.12, was introduced at the edges of the structure. This slight modification affected the configuration of the inductive irises. Subsequently, a thorough investigation was conducted to assess the impact of these curvatures on the filter parameters. It was found that the curvatures had a negligible effect on the overall filter performance. Therefore, the introduced curvatures can be safely incorporated into the manufacturing process without significantly compromising the desired filter results. The 3D models of the filters, including all the relevant dimensions, as well as the simulated S-parameter results, are presented in Figures [2.13-2.16] for reference. These figures provide a comprehensive visualization of the filter's design and performance characteristics, aiding in the understanding and evaluation of its effectiveness.

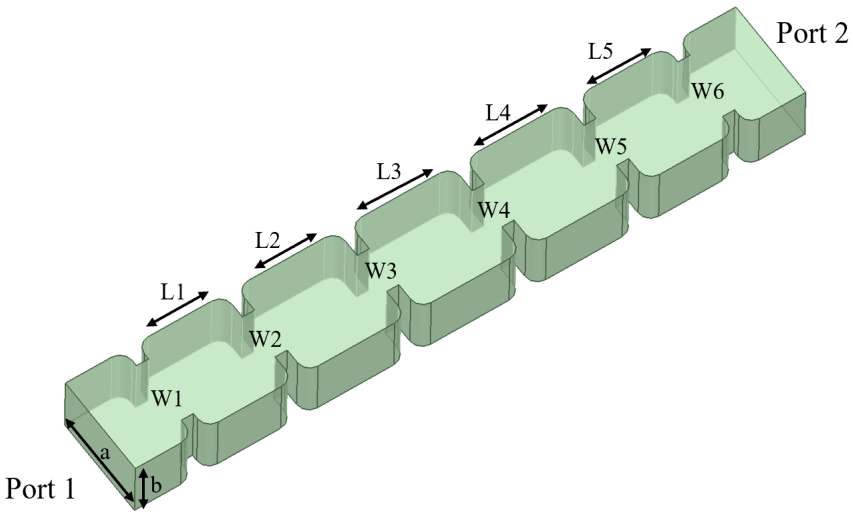

Figure 2.13: W1 sub-band filter designed using K-Impedance Inverter method; L1=L5=1.778mm, L2=L4=2.047mm, L3=2.089mm, W1=W6=1.340mm, W2=W5=0.980mm, W3=W6=0.885mm, a=2.10mm b=1.27mm

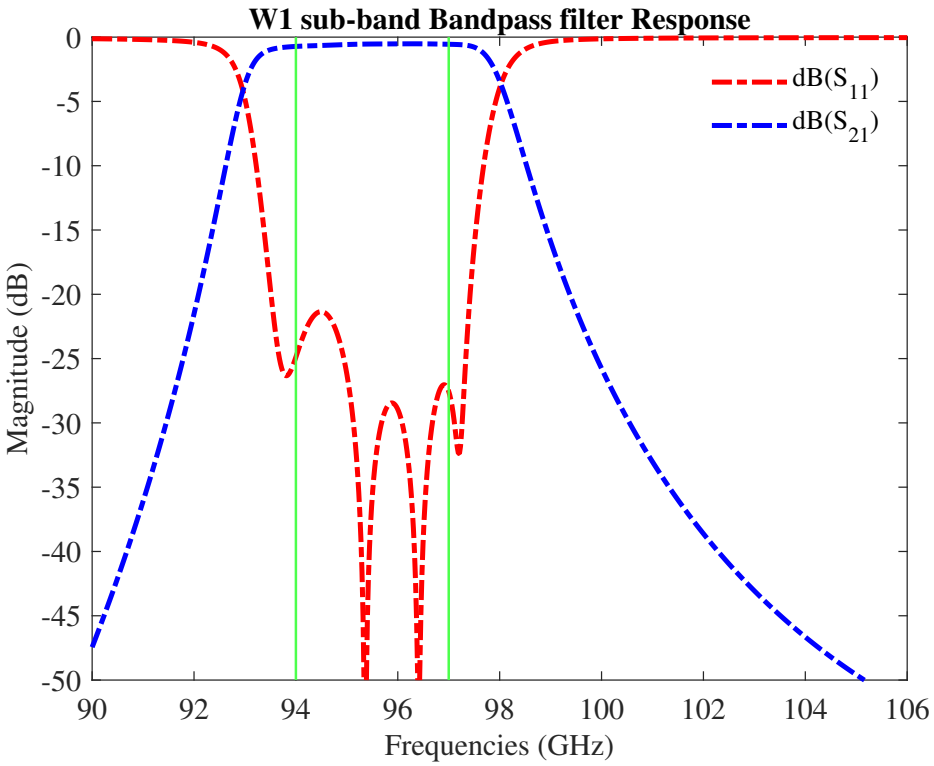

Figure 2.14: Simulated S-parameter results for W1 sub-band filter

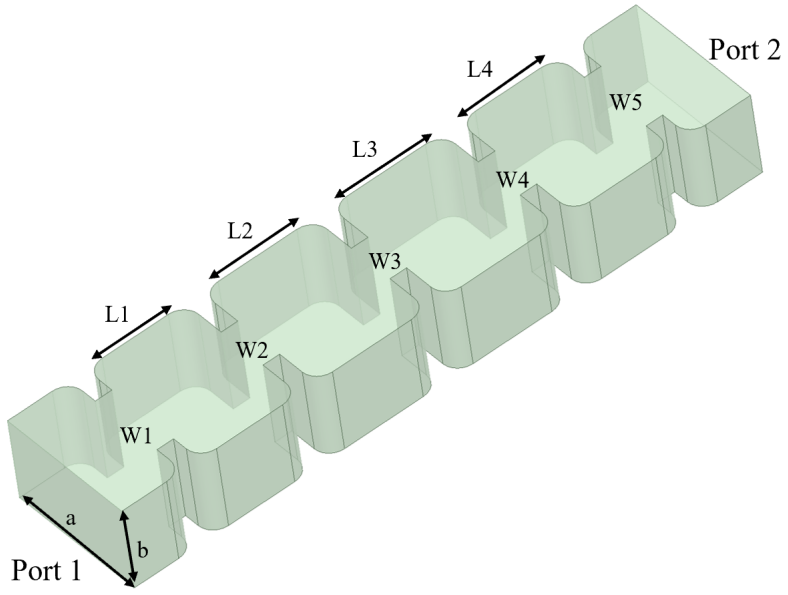

Figure 2.15: W2 sub-band filter designed using K-Impedance Inverter method; L1=L4=1.615mm, L2=L3=1.831mm, W1=W5=1.143mm, W2=W4=0.803mm, W3=0.774mm, a=1.90mm b=1.27mm

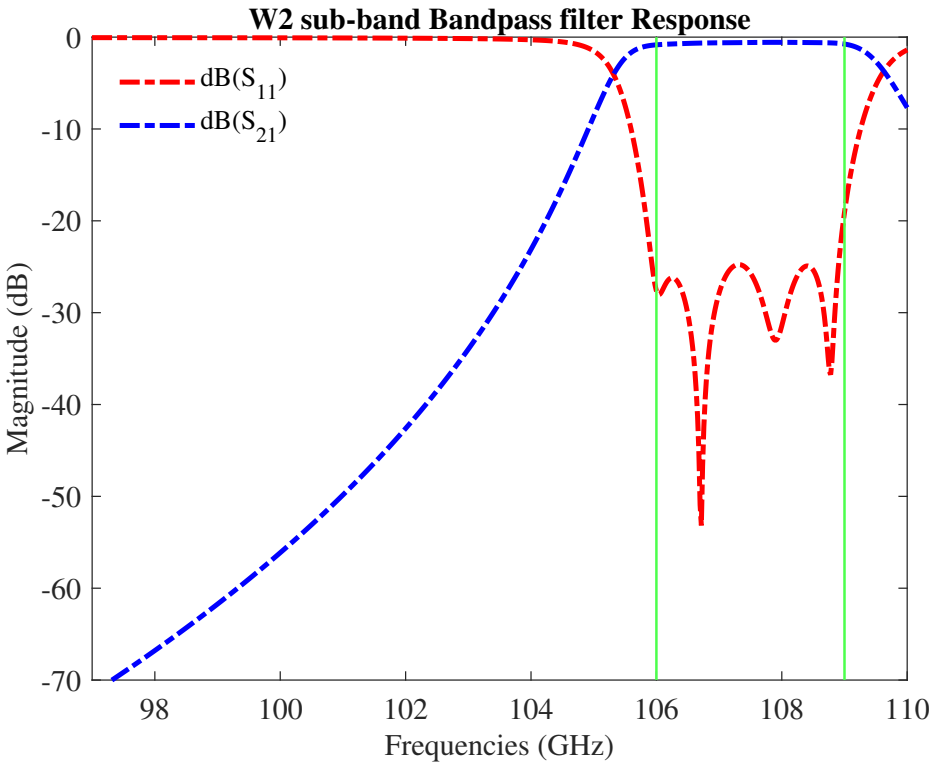

Figure 2.16: Simulated S-parameter results for W2 sub-band filter

2.4 Filter design: Coupling Matrix Model

The coupled resonator circuit can be written in the form of a matrix usually known as a coupling matrix. This coupling matrix theory has numerous advantages i.e., applying multiple matrix operations including but not limited to similarity transformation and matrix inversions during the filter design process [2] [7]. However, the coupling matrix theory is only feasible for the narrow bandwidth filters due to certain assumptions during the design process [15]. Generally, the coupling matrix method can be further classified into two categories i.e., n x n coupling matrix and n + 2 coupling matrix, where n is the order of the filter. In this section, we will briefly discuss the n x n coupling matrix method utilized for the waveguide filter design.

The coupled resonator circuit can be represented mathematically using a matrix known as the coupling matrix. The coupling matrix theory offers several advantages in the design process of filters. It allows for the application of various matrix operations, such as similarity transformations and matrix inversions, which aid in the synthesis of complex filter responses [2, 7].

However, it is important to note that the coupling matrix theory is typically applicable to narrow bandwidth filters, as certain assumptions are made during the design process [15]. There are two main categories of the coupling matrix method: the n x n coupling matrix and the n + 2 coupling matrix, where n represents the order of the filter. In this study, we will focus on the n x n coupling matrix method specifically used for the design of the waveguide filter. By employing the n x n coupling matrix

method, we can effectively analyze and design waveguide filters, taking into account the coupling between resonators and achieving the desired filter characteristics.
As mentioned earlier, this research study utilizes the Chebyshev response to demonstrate the application of filter circuit models and an electromagnetic (EM) simulator (such as HFSS) in synthesizing the physical dimensions of the filter. In Figure 2.17, the Coupling matrix circuit model for Chebyshev filters is illustrated.
Chebyshev filters are known for their ability to achieve a steeper roll-off and a sharper transition between the passband and stopband compared to other filter types. By employing the Coupling matrix method, we can effectively design Chebyshev filters, taking into account the inter-resonator coupling and achieving the desired filter response. Through the utilization of the Coupling matrix circuit model and the EM simulator, we can optimize the physical dimensions of the filter components to meet the desired specifications. This approach allows for precise control over the filter's characteristics, such as passband ripple and stopband attenuation, ensuring efficient and reliable filter performance.

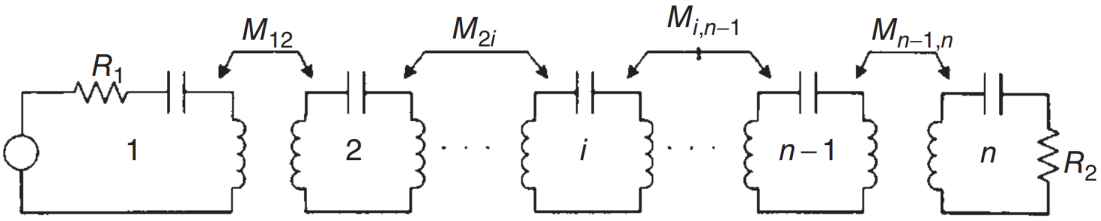

Figure 2.17: Impedance inverter model for Chebyshev filters [2]

Coupling matrix elements $M_{i,i+1}$, and external quality factors Q_{en} are related to the chebyshev lumped-element lowpass prototype elements g_0, g_1, g_2,..., g_{N+1} as expressed in [2] are as follows:

$$R_1 = \frac{1}{g_0 * g_1} \qquad R_n = \frac{1}{g_{n-1} * g_n} \tag{2.13}$$

$$Q_{e1} = \frac{f_o}{BW * R_1} \qquad Q_{en} = \frac{f_o}{BW * R_n} \tag{2.14}$$

$$M_{i,i+1} = \frac{1}{\sqrt{g_i * g_{i+1}}} \qquad for\ i = 1\ to\ n-1 \tag{2.15}$$

In the equations mentioned above BW is the passband bandwidth of the desired filter and n is the filter order. The Chebyshev lowpass prototype elements g_0, g_1, g_2, ..., g_{N+1} can be determined based on the desired filter specifications. These elements can be extracted using Equation 2.1 or by referring to Table 2.1, which provides the values corresponding to specific filter requirements.

2.4.1 Design, Optimization, and Analysis of Filter Performance

Once the coupling matrix [M] and external quality factors have been synthesized using Equations [2.13 - 2.15], the next step is to configure the waveguide cavities

with inductive irises/discontinuities based on the derived coupling matrix. This involves determining the physical dimensions of each distributed element within the filter. To accomplish this, a full-wave electromagnetic (EM) simulator such as HFSS is employed.
The EM simulator is utilized in two separate simulations, as discussed in Section 2.4.1.1 and 2.4.1.2, in order to accurately extract the filter dimensions to achieve the desired frequency response. These simulations involve configuring the waveguide cavities with inductive irises/discontinuities based on the coupling matrix and external quality factor values obtained from the previous steps.
By incorporating the EM simulator into the design process, we can fine-tune and optimize the physical dimensions of the distributed elements, ensuring that the filter meets the desired specifications and exhibits the desired frequency response. This integration of circuit models and EM simulation techniques enables precise control over the filter design, resulting in improved performance and reliability.

$$\big[M\big] = \begin{bmatrix} & 1 & 2 & 3 & 4 & 5 \\ 1 & 0 & 0.9737 & 0 & 0 & 0 \\ 2 & 0.9737 & 0 & 0.6825 & 0 & 0 \\ 3 & 0 & 0.6825 & 0 & 0.6825 & 0 \\ 4 & 0 & 0 & 0.6825 & 0 & 0.9737 \\ 5 & 0 & 0 & 0 & 0.9737 & 0 \end{bmatrix} \tag{2.16}$$

$$Q_{e1} = Q_{en} = 21.4 \tag{2.17}$$

2.4.1.1 Input/Output Coupling Elements Extraction using Q_e

There are multiple definitions for the Quality factor and we will discuss them here briefly. Unloaded quality factor Q_u is defined as the ratio of the energy stored and power lost in the reactive element per unit of time. Analytical expression for Q_u is given below:

$$Q_u = \omega * \frac{\text{E}nergy\ Stored\ in\ the\ cavity\ resonator}{\text{A}verage\ Power\ Lost} \tag{2.18}$$

The unloaded quality factor Q_u of a cavity resonator may come from the conductor loss of the cavity wall Q_c, the dielectric loss Q_d.

$$\frac{1}{Q_u} = \frac{1}{Q_c} + \frac{1}{Q_d} \tag{2.19}$$

Now coming towards the loaded quality factor i.e., Q_l, which could be extracted using both the unloaded and the external quality factor:

$$\frac{1}{Q_l} = \frac{1}{Q_u} + \frac{1}{Q_e} \tag{2.20}$$

The loaded quality factor can be extracted using the S_{21} of a single resonator as shown in Figure 2.18 using the analytical expression shown below:

$$Q_l = \frac{f_c}{BW} \tag{2.21}$$

Where f_c is the center frequency i.e., maximum peak occurrence and the BW is the 3dB bandwidth of the resonance as shown in Figure 2.18

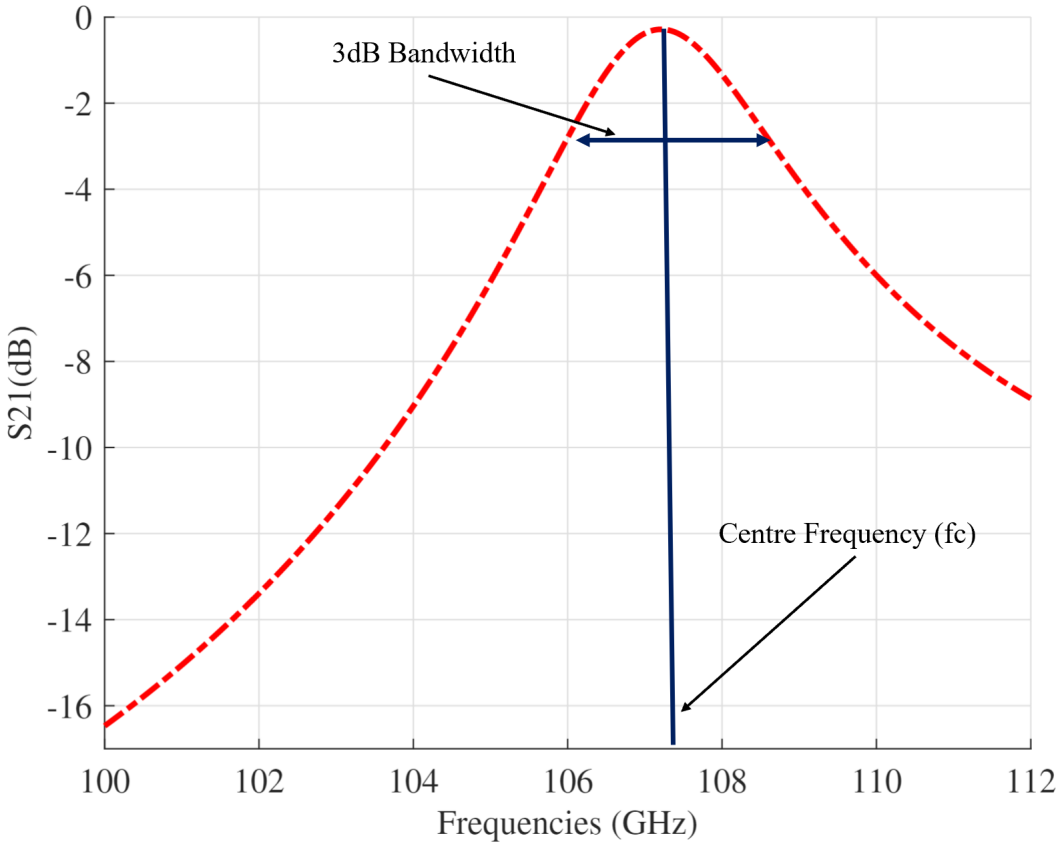

Figure 2.18: S21 plot for extraction of External Quality factor for W2 sub-band filter cavities design

In order to simplify the computations, the loaded quality factor Q_l can be made equivalent to the Q_e because in a hollow waveguide, we have no dielectric loss i.e., $Q_d \rightarrow \infty$ and we can also assume perfect conductivity thus, the simplifying the Equation 2.20 as follows:

$$Q_l = Q_e = \frac{f_c}{BW} \tag{2.22}$$

As mentioned previously we have used inductive irises with cavity resonators in order to design filters. In Figure 2.19 attached above we have used a doubly loaded cavity resonator with inductive irises on both ends which are symmetrical to each other. Thus, the quality factor computed is as follows:

$$Q_{eiris} = 2 * Q_e \tag{2.23}$$

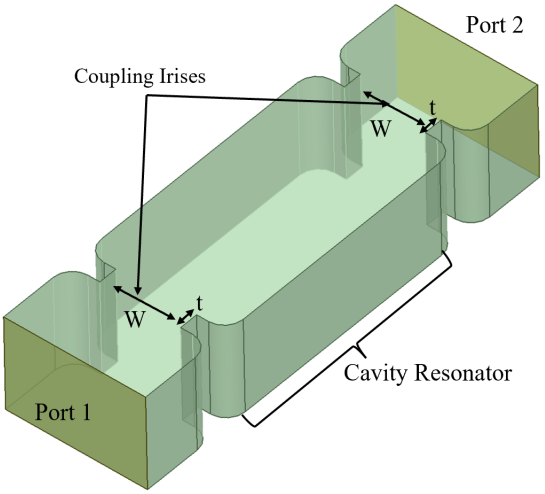

Figure 2.19: 3D-EM model of unit cell used for extraction of External Quality Factor

Keeping the iris thickness t fixed and varying the iris width W, a set of Q_{eiris} values are computed using S_{21} matrix data. Afterward, by dividing it into half, the actual values Q_e set can be stipulated. The relationship between the iris width W and Q_e is illustrated in Figure 2.20.

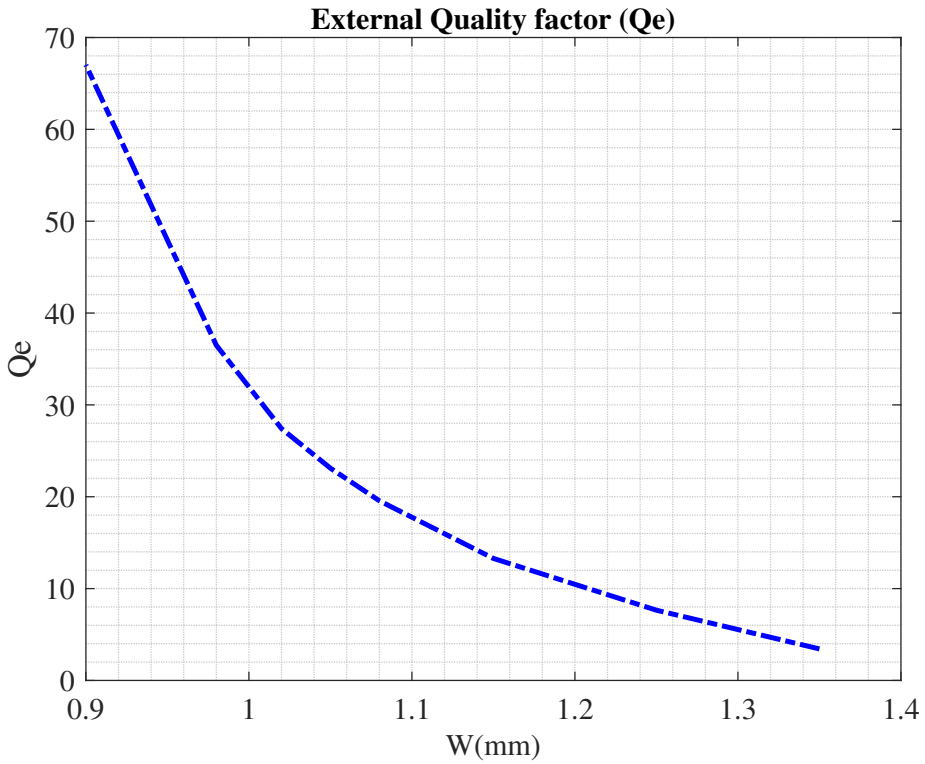

Figure 2.20: External quality factor (Q_e) vs iris window width (W) for the waveguide structure shown in Figure 2.19

During the design process, an important consideration is an adjustment of the cavity resonator length and the width of the irises (denoted as W). By manipulating these parameters, it is possible to tune the resonance frequency of the cavities and ensure that the quality factor matches the desired value obtained from equation 2.14. It should be noted that this adjustment process requires iterative simulations and optimizations using an EM simulator. By analyzing the simulated results and comparing them to the desired specifications, the dimensions can be fine-tuned to achieve the desired resonance frequency and quality factor. This iterative approach ensures that the filter meets the desired performance requirements and provides accurate and reliable filtering characteristics.

2.4.1.2 Inter-resonator coupling elements extraction

The internal coupling coefficient between resonators could be an electric, magnetic, or mixed coupling. In this work, we have considered the coupled resonators are synchronously tuned i.e., their resonant frequencies are the same. One approach to extracting the inter-resonator coupling is to use electric and magnetic wall symmetry. This involves dividing the problem into single resonators terminated by a magnetic wall and an electric wall and determining the coupling based on the resonant frequencies (f_e and f_m) of the individual resonators [2]. The approach based on electric and magnetic wall symmetry necessitates the use of an electromagnetic simulator that can perform eigenvalue calculations, such as HFSS. A different approach to determine the resonant frequencies f_e and f_m is by connecting the two resonators in a two-port network configuration as illustrated in Figure 2.21. It is important to ensure that the ports are weakly coupled to the resonator for accurate results. The sketch of return loss (S_{11}) is provided in Figure 2.22 where the two dips represent the two frequencies f_e and f_m [2].

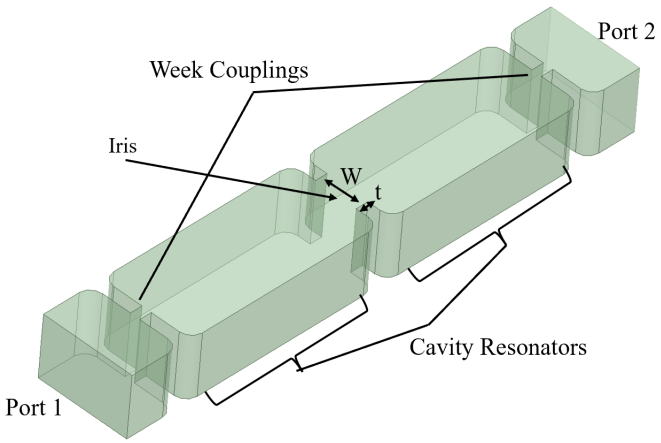

Figure 2.21: 3D-EM model of unit cell used for extraction of Interresonator couplings

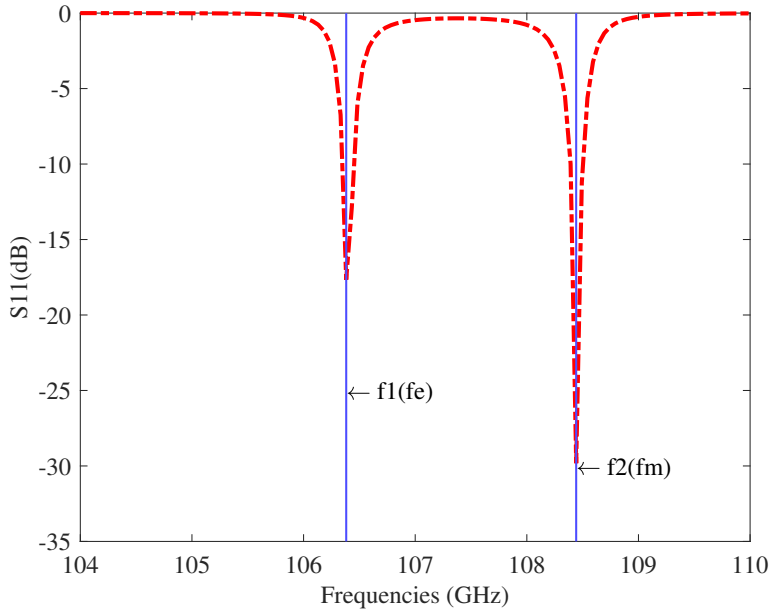

Figure 2.22: The return loss of the waveguide structure shown in Figure 2.21

The physical coupling elements ($k_{i,j}$) are computed (Equation 2.24) using the resonant frequencies, which are then related to the coupling matrix elements ($M_{i,j}$) given by Equation 2.25.

$$k_{i,j} = \frac{f_e^2 - f_m^2}{f_e^2 + f_m^2} \tag{2.24}$$

$$M_{i,j} = \frac{f_0}{BW} * k_{i,j} \tag{2.25}$$

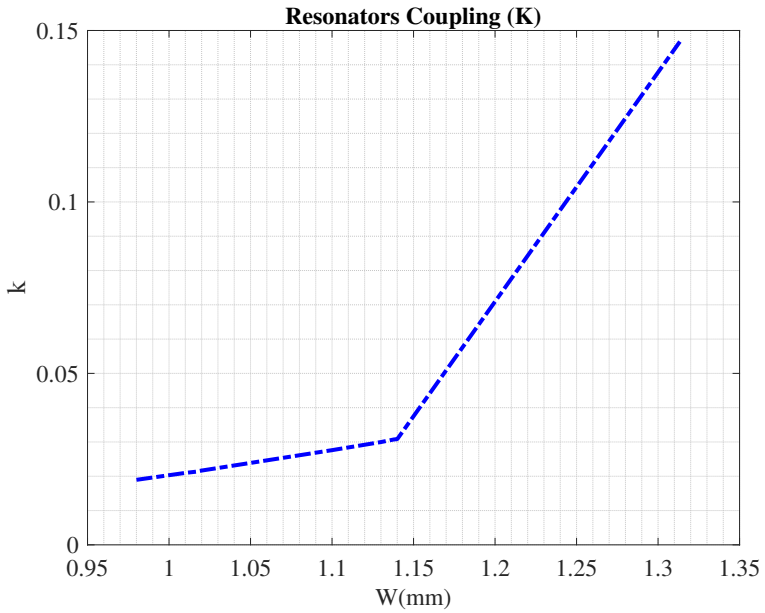

Figure 2.23: Resonator coupling (k) versus iris window (W) calculated using the equations 2.24 and simulation illustrated in Figure 2.21

Based on Figure 2.23, we can accurately derive the iris dimensions (W1-W6; visualized in Figure 2.9) needed to attain the predetermined coupling elements, M_{12}, M_{23}, and M_{34} as outlined in 2.16 using equations 2.15.

The half-wave cavity filter designed using the Coupling Matrix method demonstrates similar dimensions and performance compared to the previous approach using the K-Impedance inverter method. However, the Coupling Matrix method offers more flexibility that allows for greater control and optimization of the filter's performance, which can be advantageous in certain applications. This method is particularly suitable for designing more complex filters i.e., cross-coupled and adding transmission zeros, etc.
Overall, the Coupling Matrix method provides a powerful and versatile approach to filter design, offering wider bandwidths and the ability to incorporate higher-order modes. It enables the realization of filters with desired performance characteristics while maintaining comparable dimensions to other design methods.

2.5 Sensitivity Analysis for Waveguide Filters

Sensitivity analysis, also known as tolerance analysis, is a crucial process performed in the manufacturing industry to assess the impact of geometric variations on the performance of waveguide filters. It helps determine the allowable variation in dimensions while maintaining the desired performance. Conducting sensitivity analysis during the design phase is essential to ensure that manufacturing errors do not compromise the overall performance of the filters, especially when producing them in high volumes. Incorporating design techniques that relax tolerance allowances for manufacturing errors is necessary and should be established in advance to ensure a smooth manufacturing process. However, achieving a robust design that can withstand manufacturing errors can be challenging, even for simple assemblies, and precision manufacturing can incur significant costs. Therefore, employing different tolerance analysis approaches and methods based on the critical requirements of the assembly becomes essential. These approaches can save valuable time and costs by enabling the design, build, assembly, and testing of modules in a more robust and effective manner.
Various techniques, including sensitivity analysis, statistical analysis, and parametric sweep, can be employed using an electromagnetic (EM) simulator such as HFSS to perform tolerance analysis. In this research work, a parametric sweep model for tolerance analysis using HFSS was employed for W1 and W2 sub-band filters. Through careful analysis, it was observed that a few parts in the assembly were highly sensitive to variations, and the maximum tolerance allowance was determined to be $\pm 15um$, which falls within acceptable limits in standard industrial manufacturing. Figures 2.24 and 2.25 exhibit the variation in simulated S-parameters performance of the W1 sub-band filter in relation to dimensional fluctuations in resonator lengths and irises opening widths, respectively. However, there are multiple methods available to reduce the sensitivity of waveguide filters, which will be discussed in detail in the subsequent sections.

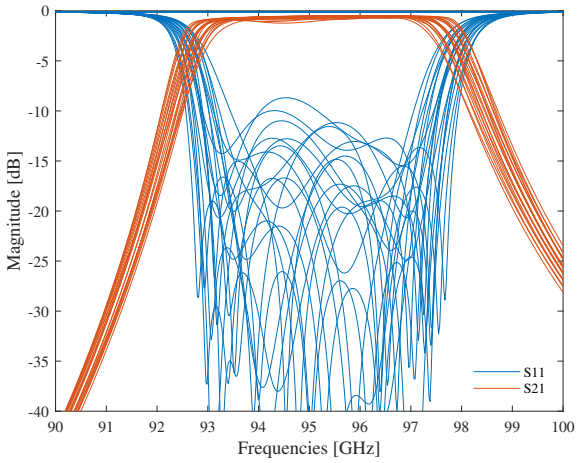

Figure 2.24: Simulated S-parameter results for W1 sub-band filter by varying the Resonator lengths within a range of $\pm 15um$

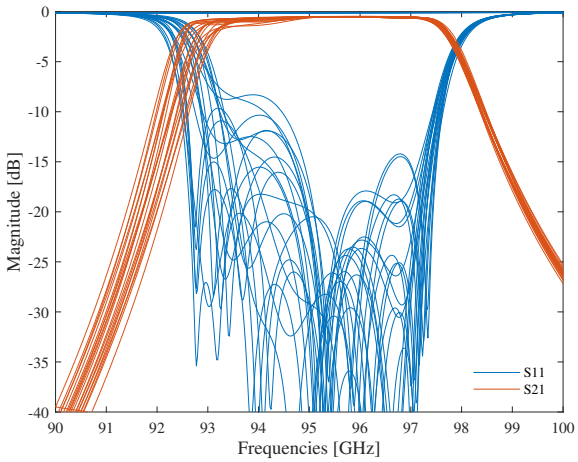

Figure 2.25: Simulated S-parameter results for W1 sub-band filter by varying the Irises opening window within a range of $\pm 15um$

2.6 Optimizing Design Tolerance for Waveguide Filters: Techniques and Strategies

Waveguide filters are crucial components in modern communication networks, especially in satellite communication and radio/TV broadcasting [2]. They use a series of stacked resonators to form a complete rectangular waveguide filter. One significant advantage of waveguide filters is their relatively small footprint, making them well-suited for mobile and space applications with size constraints [8]. However, to maintain these advantages, it's essential to ensure that the manufacturing process is both straightforward and cost-effective. The main cost driver for waveguide filters is the need for precise manufacturing, which is closely linked to design sensitivity. To address this challenge, various methods can be employed to improve design sensitivity and reduce manufacturing errors. These approaches will be thoroughly explored

in the following sections

2.6.1 Higher Order Mode (TE_{10n},n≥2) Filters

Waveguide filters designed for W-band operation are compact due to their small component size. However, the close placement of resonators in the structure leads to a high degree of interconnectivity and dependency between different elements, resulting in significant design sensitivity. To mitigate this sensitivity, one approach is to increase the overall volume of the filters by extending the length of resonator cavities to multiples of half-wavelengths (e.g., λ_g or $\frac{3\lambda_g}{2}$), creating higher-order mode filters. These filters effectively reduce the interdependence between elements, thereby reducing design sensitivity. The resonance cavity is illustrated in Figure 2.6 and discussed in detail in Section 2.2.2.
Waveguide filters designed for W-band operation are known for their compact size, due to the small dimensions of the individual components. However, this compactness comes at the cost of increased design sensitivity. Due to the close placement of resonators in the filter structure, there is a high degree of interconnectivity and dependency between different elements, making the filter performance highly sensitive to dimensional variations. To address this design sensitivity, one effective strategy is to increase the overall volume of the filters. This can be achieved in three ways: increasing the length of the resonators, increasing the waveguide width, or increasing the waveguide height. However, in the TE_{10} mode of operation, the waveguide's height and width are usually standardized and cannot be varied significantly. Therefore, increasing the length of the resonators to a multiple of half-wavelengths, such as λ_g or $\frac{3\lambda_g}{2}$ is often the most feasible solution. By doing so, the filter operates in a higher-order mode, which reduces the interdependence between the elements and mitigates the design sensitivity. The concept behind this approach lies in the fact that by increasing the size of the resonator cavities, the electromagnetic field distribution within each cavity becomes less affected by the adjacent cavities and their dimensions. This reduction in interdependence leads to improved tolerance against manufacturing variations and dimensional errors.

2.6.2 Resizing of sensitive resonators from $\frac{\lambda_g}{2}$ to λ_g

Waveguide bandpass filters are commonly designed using half-guided wavelength $\frac{\lambda_g}{2}$ resonators, striking a balance between filter performance and size. However, employing full-wavelength $\frac{\lambda_g}{2}$ resonators for the complete filter as discussed in section 2.6.1 can be a more effective approach for reducing design sensitivity. Nonetheless, this method introduces challenges as it may cause spurious responses near the filter's passband, which is an undesirable phenomenon [3]. To reduce sensitivity without spurious responses, targeting the sensitive resonator (often the central one) is an alternative strategy [3]. This involves doubling the size of the critical resonator to operate as a full-wavelength while keeping the remaining resonators at the half-wavelength size. By increasing the size of this cavity, the sensitivity of the critical resonator is reduced. The aperture size of the input and output coupling irises

also needs to be increased to accommodate the full-wavelength resonator, further decreasing the manufacturing sensitivity of the critical irises. It's important to note that increasing the aperture size is necessary because the full-wavelength resonator stores more energy than the half-wavelength resonator due to its larger volume. This approach provides a better trade-off in terms of sensitivity, size, and performance parameters of waveguide filters.

2.6.3 Capacitive rectangular waveguide structures

Capacitive irises are frequently employed in waveguide structures that operate along the E-field and are commonly used in the design of low-pass filters, impedance converters, and matching networks [7, 20]. Unlike inductive irises, capacitive structures induce a positive length in the resonator as illustrated in Figure 2.26, allowing for increased volume and size of the cavities. This characteristic reduces sensitivity to manufacturing variations. Another advantage of capacitive discontinuities is their logarithmic increase in capacitance with changes in the height of the discontinuity, leading to decreased sensitivity to variations. Asymmetric capacitive irises are commonly employed to ensure manufacturing simplicity, which offers additional advantages.
However, incorporating capacitive irises presents several challenges i.e., in configurations with a small number of resonators, the coupling requirements between adjacent resonators are significantly reduced, necessitating very small openings in the discontinuity [21]. Machining such small openings can be challenging compared to inductive irises, which require larger openings. The other challenge could be that in high-power applications, waveguide resonator filters with capacitive or E-plane discontinuities are prone to breakdown due to E-field concentration [22]. These factors contribute to the limited use of capacitive irises in waveguide structures.

(a) **(b)**

Figure 2.26: Waveguide Irises:(a)Capacitive Iris (b)Inductive Iris [3]

2.7 Higher order modes filters and cavities design

Based on the comprehensive comparative analysis between different strategies presented in the preceding sections, it has been established that incorporating higher-order mode filters or introducing higher-order mode cavities within the filter struc-

ture is the optimal approach to mitigate design sensitivity to manufacturing variations. The subsequent sections elaborate further on the finalized strategies, design methodology, and corresponding results.

2.7.1 Resizing of sensitive resonator from $\frac{\lambda_g}{2}$ to λ_g

The theory of direct coupled bandpass filters has been previously discussed in Section 2.1. Symmetrical inductive irises, as illustrated in Figure 2.7, are employed as the discontinuity structure within the waveguide filter body. Initially, $\frac{\lambda_g}{2}$-sized five-pole (W1 sub-band) filter is designed through the implementation of the K-impedance inverter method. An EM-simulator-based optimization routine is then employed to achieve the desired performance specifications for the filter, utilizing the determined dimensions. After conducting a parametric sweep analysis using HFSS, the third (central) resonator, was identified as the most sensitive resonator. Thus its length is doubled to λ_g and subsequent tuning of the filter parameters is performed accordingly. The figures below showcase the 3D model of this designed filter.

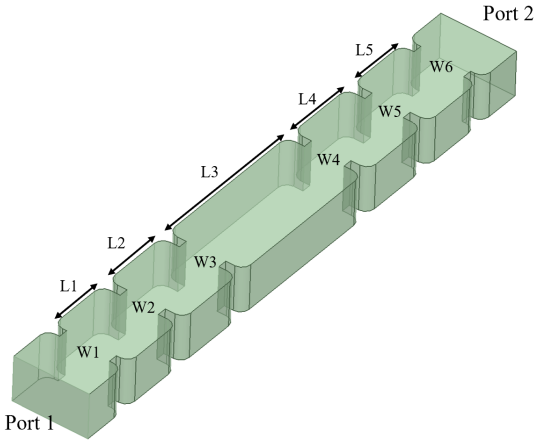

Figure 2.27: W1 sub-band filter with central cavity λ_g; L1=L5=1.173mm, L2=L4=1.927mm, L3=4.301mm W1=W6=1.38mm, W2=W5=1.06mm, W3=W4=1.095mm

2.7.2 TE_{102} mode filters design

TE_{102} mode filters, are designed by employing full-wavelength λ_g cavity resonators instead of the conventional half-wavelength $\frac{\lambda_g}{2}$ resonators. In this approach, λ_g-sized five-pole W1 sub-band and four-pole W2 sub-band filters are designed using the coupling matrix method. This results in an increased overall volume of the filters compared to the previous case, necessitating an enlargement of the aperture size of the inductive irises to accommodate the energy storage requirements of the full-wavelength resonator architecture. The figures below depict the 3D model and simulated frequency response of the designed filters.

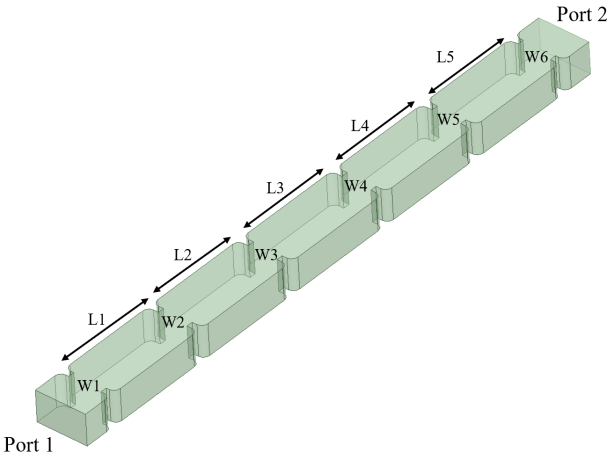

Figure 2.28: TE_{102} mode W1 sub-band filter; L1=L5=4.011mm, L2=L4=4.246mm, L3=4.301mm, W1=W6=1.446mm, W2=W5=1.173mm, W3=W4=1.103mm

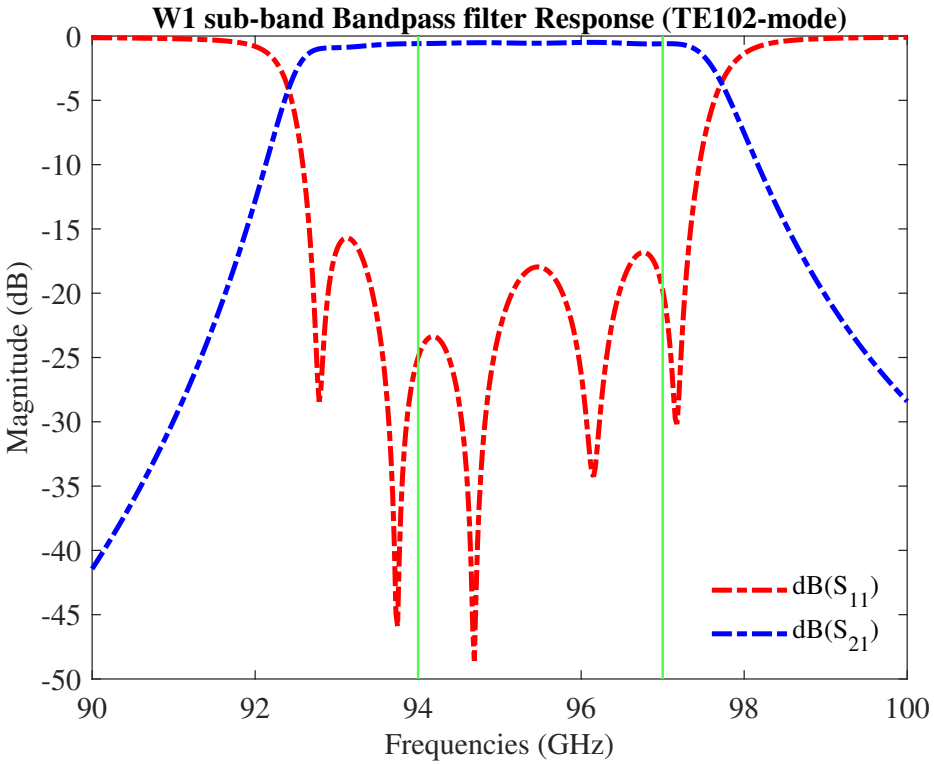

Figure 2.29: Simulated S-parameter results for TE_{102} mode W1 sub-band filter

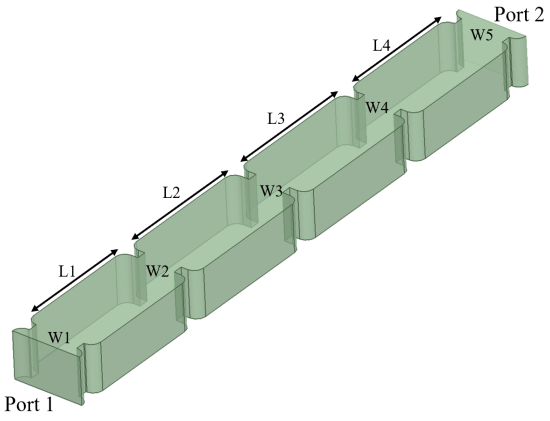

Figure 2.30: TE_{102} mode W2 sub-band filter; L1=L4=3.446mm, L2=L3=3.692mm, W1=W5=1.337mm, W2=W4=1.026mm, W3=0.948mm

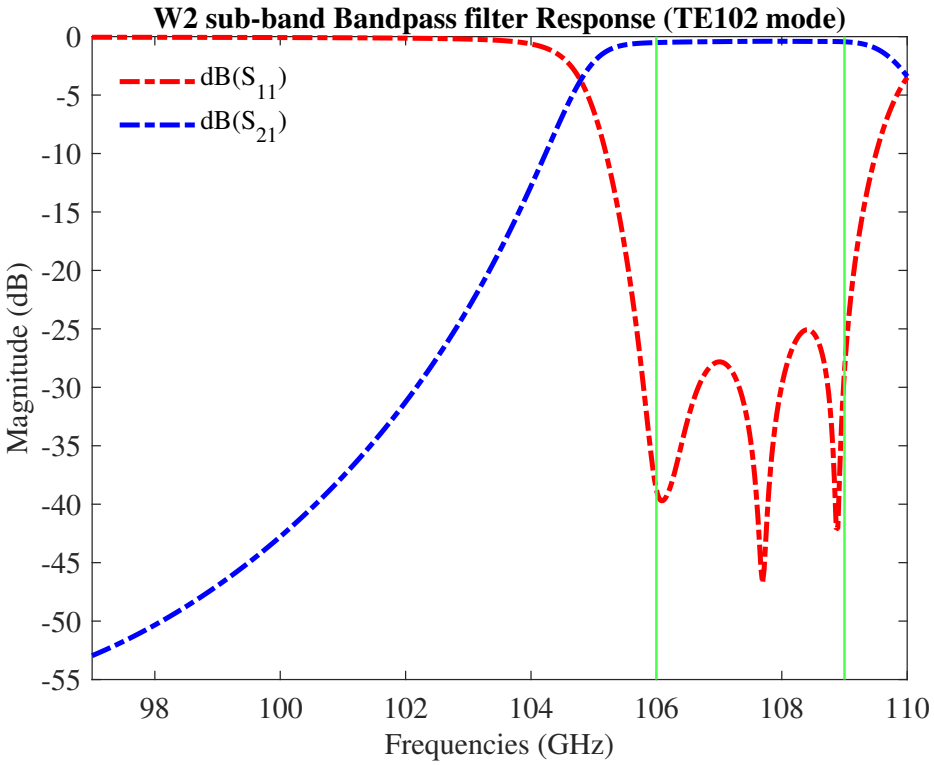

Figure 2.31: Simulated S-parameter results for TE_{102} mode W2 sub-band filter

2.7.3 TE_{103} mode filters design

Similarly, TE_{103} mode filters are designed by using the $\frac{3\lambda_g}{2}$ cavity resonators instead of traditional half-wavelength $\frac{\lambda_g}{2}$ resonators. In this method, initially, five-pole W1 sub-band and four-poles W2 sub-band filters are designed using the coupling matrix method. This will increase the overall volume of the filters compared to the previous case, and the aperture size of inductive irises is also increased in order to

accommodate $\frac{3\lambda_g}{2}$ resonator architecture. The 3D model and simulated frequency response of the filters are shown in the figure below:

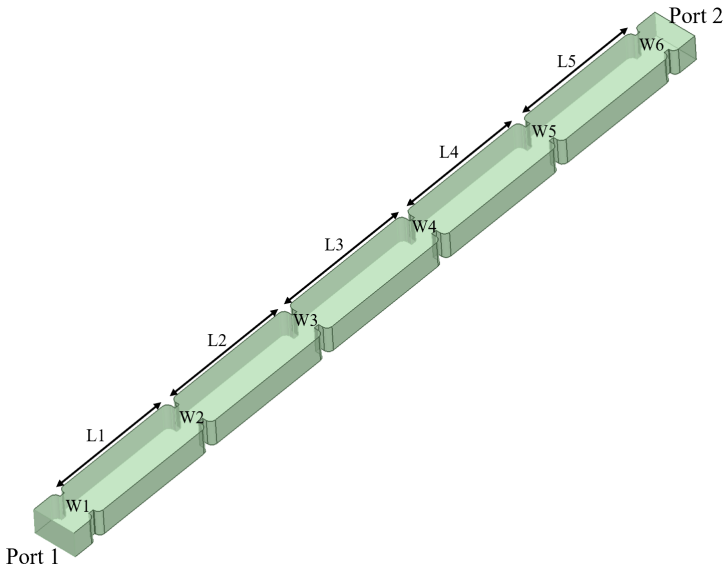

Figure 2.32: TE_{103} mode W1 sub-band filter; L1=L5=6.263mm, L2=L4=6.518mm, L3=6.572mm, W1=W6=1.508mm, W2=W5=1.219mm, W3=W4=1.134mm

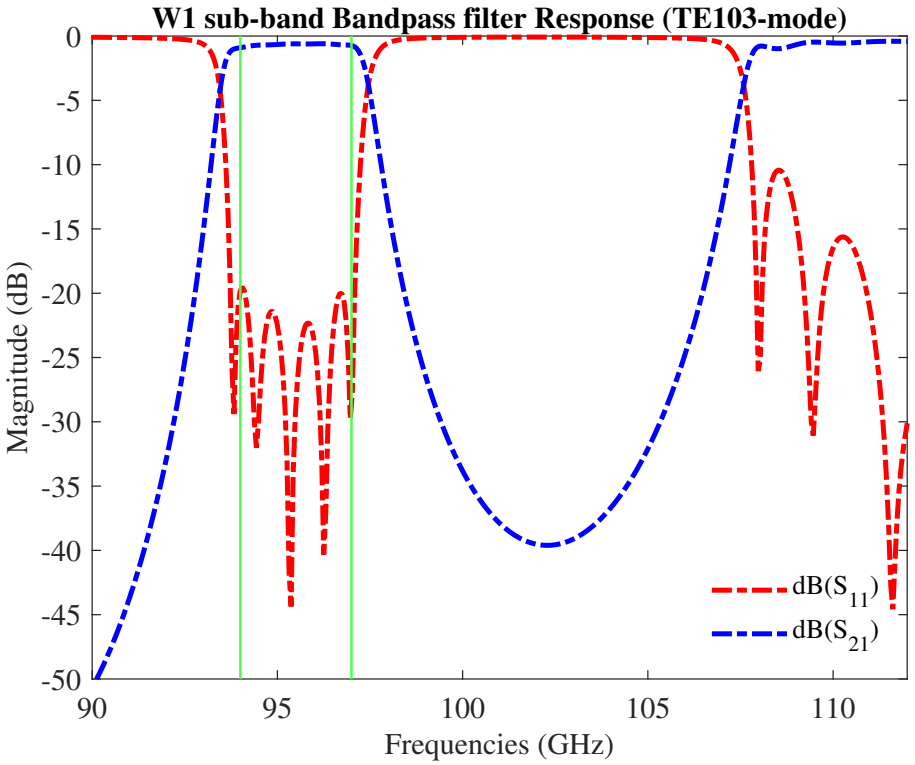

Figure 2.33: Simulated S-parameter results for TE_{103} mode W1 sub-band filter

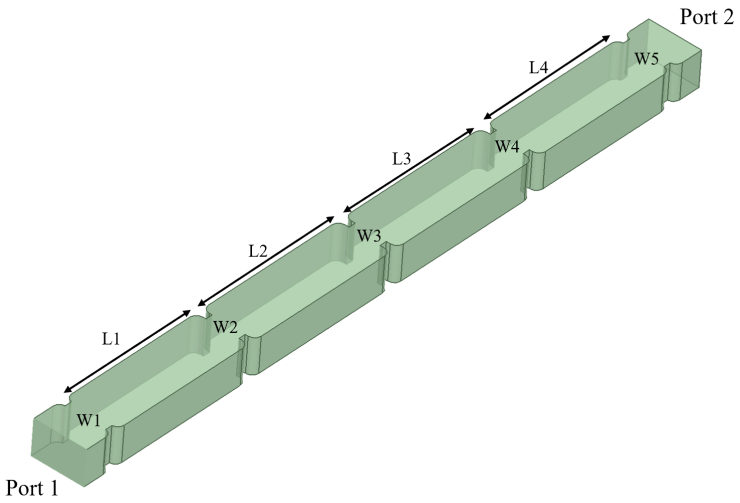

Figure 2.34: TE_{103} mode W2 sub-band filter; L1=L4=5.30mm, L2=L3=5.509mm, W1=W5=1.45mm, W2=W4=1.186mm, W3=1.114mm

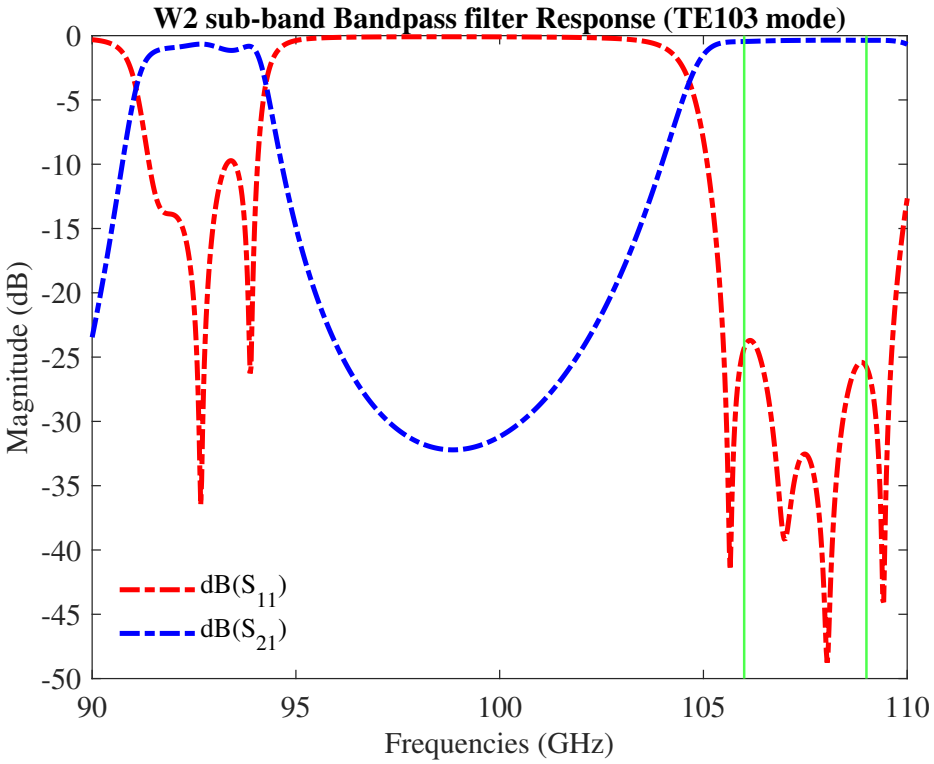

Figure 2.35: Simulated S-parameter results for TE_{103} mode W2 sub-band filter

Upon analyzing the frequency response of TE_{103} mode filters, it was noted that they exhibit resonance in both the desired sub-bands. This particular behavior renders TE_{103} mode filters unsuitable for our Diplexer design. Typically, odd-mode cavity filters are designed for dual-band operations. However, the resonance characteristics of TE_{103} mode filters in both sub-bands render them incompatible with the intended FDD operations.

3

Diplexer Implementation and Performance Analysis

3.1 Introduction

Diplexers are essential components in wireless backhaul links, incorporating various modules such as T-junctions and filters [23, 24]. They play a critical role in point-to-point communication links by enabling the separation of transmit (TX) and receive (RX) signals, thus facilitating a Frequency Division Duplexing (FDD) configuration. Figure 3.1 visually depicts a conceptual block-level diagram of a diplexer. In this specific research project, which focuses on the design of a W-band diplexer assembly, the duplexing is accomplished using two bandpass filters. Additionally, there are two potential options for the T-junction design: E-plane or H-plane T-junction. Notably, the filter design remains consistent in both cases, with the variation being solely in the placement of the filters.

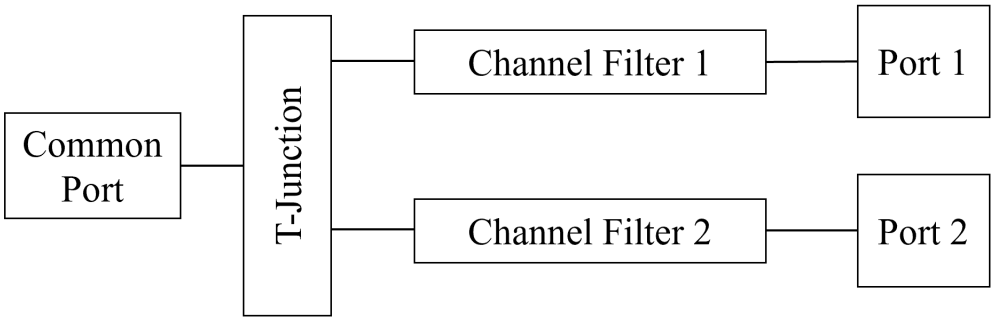

Figure 3.1: Block Diagram of a Diplexer

3.2 T-Junction and its types

The design of the T-junction is a critical factor in achieving optimal performance for the diplexer assembly. Figures 3.2a and 3.2b illustrate two different types of T-junctions: E-plane and H-plane T-junctions. The selection of the junction type takes into consideration several factors, including the cutoff frequencies of different

propagation modes, the overall size of the diplexer assembly, and the ease of integration within the complete antenna system. For the specific application at hand, the T-junction is required to have a bandwidth of approximately 15 GHz, spanning from 94 GHz to 109 GHz. Furthermore, the diplexer assembly needs to be integrated with a Focal plane array, a compact power combiner, and a beamforming network, necessitating an overall reduction in size. In light of these considerations, the H-plane T-junction is chosen for the diplexer configuration in this study.

(a) E-plane waveguide T **(b)** H-plane waveguide T

Figure 3.2: Waveguide T-junction Types

3.2.1 H-plane T-junction Design

To achieve an optimal diplexer design, it is recommended to initially focus on designing the T-junction separately before integrating it with the bandpass filters. This approach allows for a better understanding of the required efforts to achieve the desired performance. This section specifically addresses the main challenge of diplexer design, excluding the filters, to provide insights into the necessary considerations.
When designing the H-plane T-junction, two potential options are available. One option involves using reduced-height T-junctions that are matched with ports using waveguide transformers [25]. Alternatively, a simpler configuration can be pursued by employing full-height H-plane T-junctions without transformers. However, it is important to note that full-height T-junction configurations are commonly used in manifold setups [26], which may be susceptible to spurious resonances and exhibit a poor input reflection coefficient [27]. For this particular design process, a conventional full-height H-plane T-junction, depicted in Figure 3.2b, is employed while adhering to the desired specifications. This selection ensures compatibility with the overall diplexer design objectives

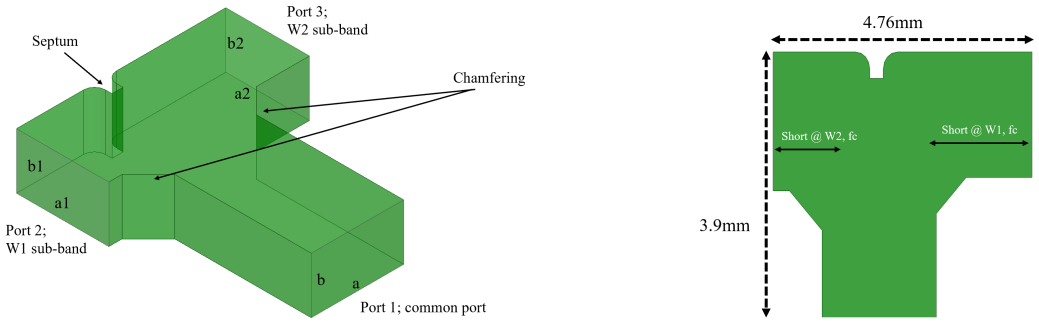

(a) **(b)**

Figure 3.3: 3D-EM model of H-plane T-junction; a=a1=2.1mm, a2=1.9mm, b=b1=b2=1.27mm

The design process of the H-plane T-junction followed a commonly employed methodology, which involved incorporating a wedge (Septum) in the center of the junction, as depicted in Figure 3.3. The precise positioning and length of the wedge play crucial roles in determining the diplexer's performance parameters. However, due to CNC milling manufacturing constraints, the width of the wedge was maintained at a constant value of 250um.
To achieve the desired frequency response, we optimized both the input waveguide and the arms of the T-junction by employing an impedance manipulation strategy. Symmetrical chamfers were also introduced to minimize reactance at the corners of the T-junction. Through multiple iterations, all parameters were carefully adjusted to attain the desired performance of the diplexer assembly.
To streamline the simulation process and save computational time, we implemented an EM-circuit co-simulation strategy using HFSS to extract initial design parameters. This approach is elaborated upon in Section 3.3.1.1, which provides detailed information on the EM-circuit co-simulation strategy utilized in this design work.

3.3 Diplexer Assembly Design

To ensure optimal performance of the diplexer and filters, it is crucial to consider manufacturing tolerances during the design process. In Section 2.4, various strategies are proposed to mitigate the sensitivity of the design to these tolerances. One approach employed in this research thesis is the utilization of higher-order mode cavities or filters [28] [3]. This technique has proven effective in reducing the impact of manufacturing tolerances on the overall design.
Throughout the diplexer design process, several configurations were evaluated to assess their ability to minimize design sensitivity to manufacturing tolerances. In this section, three of these configurations are comprehensively discussed. Each configuration was thoroughly analyzed and evaluated based on its effectiveness in reducing sensitivity and its impact on the overall volume of the diplexer. Through this analysis, the most suitable design configuration was identified for manufacturing and subsequent integration into the antenna system. The finalized design exhibited the

highest effectiveness in reducing sensitivity to manufacturing tolerances, while also maintaining a reasonable overall volume for the diplexer.

3.3.1 TE_{101} mode Diplexer Design

The fundamental approach is to design a diplexer by utilizing TE_{101} mode filters, which involves designing cavity resonator filters with a size of $\lambda_g/2$. Chapter 2 provides a thorough discussion on filter design. In this section, design and optimization methodologies for diplexers are discussed and analyzed

3.3.1.1 EM-circuit co-simulation

The term "co-simulation" refers to a simulation technique that involves multiple simulation types working together to model a complete system. This can be done either in a serial analysis, where the output of one simulation is fed into another tool for further analysis or in a coupled simulation, where the tools exchange data bi-directionally in a dynamic linking scenario. In this particular design, individual electromagnetic (EM) simulations are carried out for the bandpass filters (W1 and W2 sub-bands) and the T-junction, and then the results are incorporated into the HFSS circuit simulation to obtain the integrated performance [29]. This process effectively reduces the simulation time and provides a convenient way to extract initial design parameters. The EM-circuit co-simulation environment is depicted in Figure 3.4.

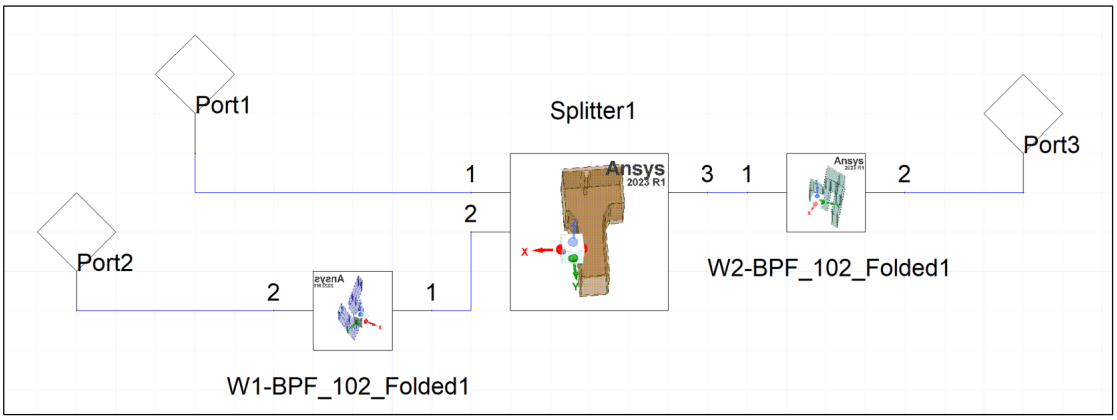

Figure 3.4: Snapshot of EM-circuit cosimulation setup from HFSS

3.3.1.2 3D-EM Model Design and Optimization

As discussed in the previous section, the initial design parameters of the diplexer are extracted from the EM circuit co-simulation technique. Afterward, the 3D-EM model as shown in Figure 3.5 of complete diplexer assembly is designed in HFSS for performance validation and further optimizations. The diplexer design aimed in this project has an overall bandwidth of 14.7%, with the bandwidths of individual

filters being less than 4%.

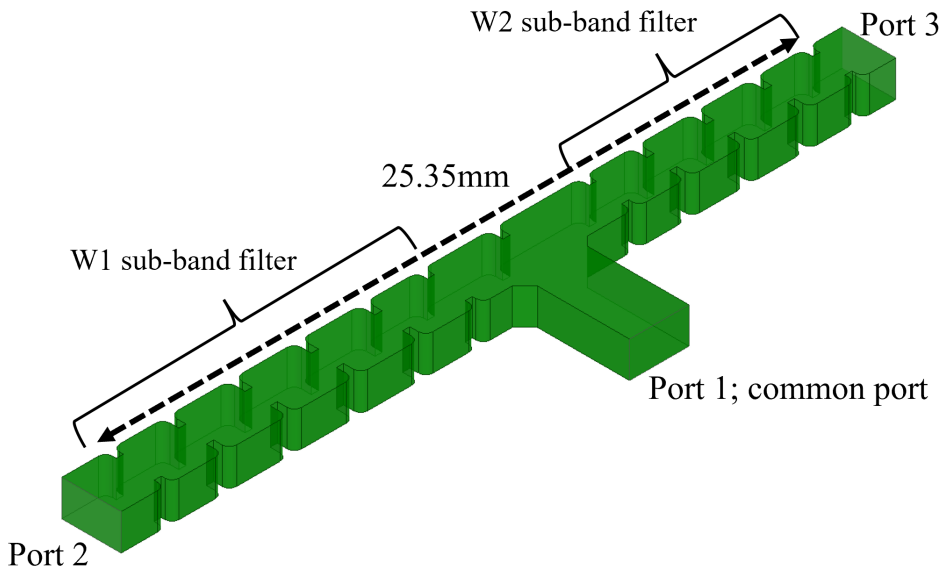

Figure 3.5: TE_{101} mode Diplexer 3D-EM model

Upon initial evaluation, it was observed that the EM simulation S-parameter results differed from the circuit simulations. This disparity is expected since the circuit simulation relies on independent S-parameters at the output ports. However, in a 3D-EM model, the entire structure is interconnected, which may introduce impedance variations and potentially impact the performance of the diplexer. To address this, both manual and cost-function-based optimization routines were implemented, with a specific focus on optimizing the T-junction parameters.

The simulated S-parameter results for the TE_{101} mode diplexer are presented in Figure 3.6, showcasing the achieved performance. Furthermore, a summary of the simulated parameters is provided in Table 3.1. These results demonstrate the effectiveness of the optimization techniques employed to improve the performance of the diplexer assembly and align the simulated parameters with the desired specifications.

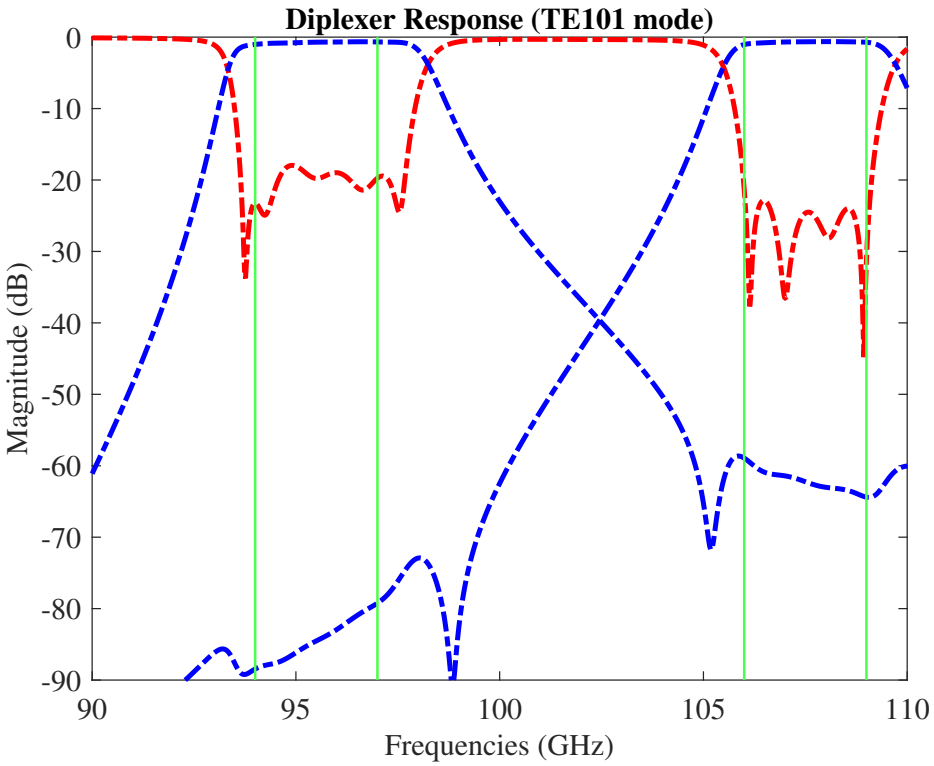

Figure 3.6: Simulated S-parameters for the TE_{101} mode diplexer design

Table 3.1: Diplexer simulated parameters

Diplexer	Specifications
Bandpass filter channel 1	94-97 GHz
Bandpass filter channel 2	106-109 GHz
Return loss	$\leq$-18dB
Insertion loss	<1dB
Isolation between two channels	better than 60dB

3.3.2 Custom configuration Diplexer Design

This second configuration design approach involves modifying the TE_{101} mode diplexer by targeting and increasing the size of the most sensitive resonators in the entire assembly. During the sensitivity analysis of TE_{101} mode diplexer, it is learned that the central cavity of the W1 sub-band filter and all four cavities of the W2 sub-band filter are sensitive to dimensional variations.
The method proposed here is considered feasible as it involves increasing the length of the most sensitive center resonator in the bandpass filter to the full wavelength size. This helps to decrease the sensitivity to fabrication errors that may arise due to changes in the resonator length. Additionally, this approach does not introduce

any spurious responses [3]. Thus the size of the center-most resonator of the W1 sub-band filter and all four resonators of the W2 sub-band filter is doubled, from $\frac{\lambda_g}{2}$ to λ_g, and the input/output coupling irises for these resonators were also optimized accordingly.

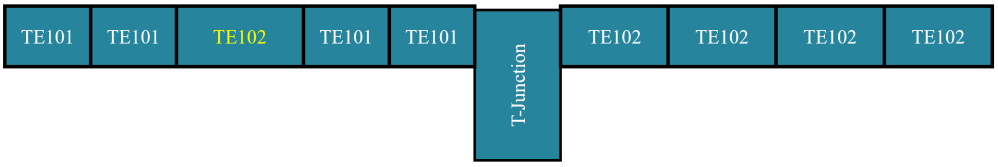

Figure 3.7: Block diagram for custom configuration of diplexer

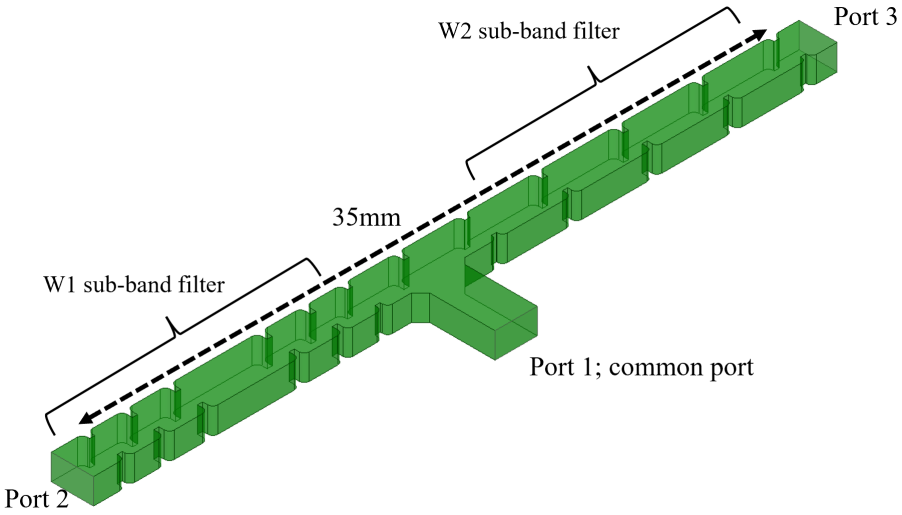

Figure 3.8: Custom configuration diplexer 3D model

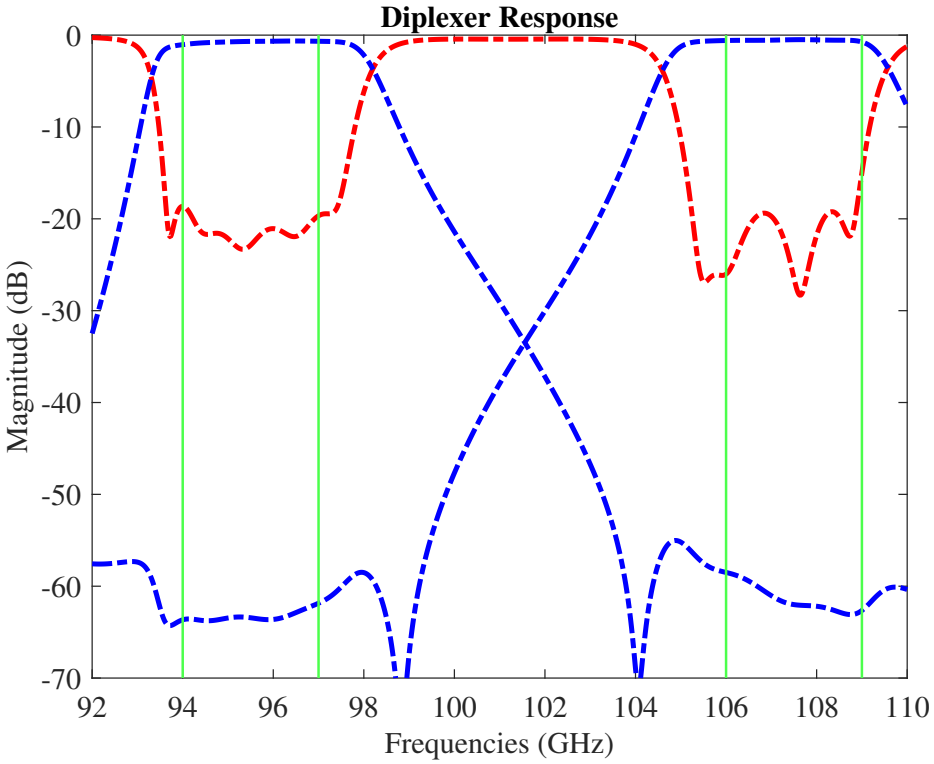

Figure 3.9: Simulated S-parameters for the custom configuration diplexer design

3.3.3 TE_{102} Diplexer Design

The diplexer design discussed in this section is based on TE_{102} mode filters, and it was developed using a design methodology similar to the one described in 3.3.1. The initial parameters were extracted through EM-circuit co-simulation, and then a 3D-EM model for the complete assembly was designed and optimized to meet the desired performance requirements.

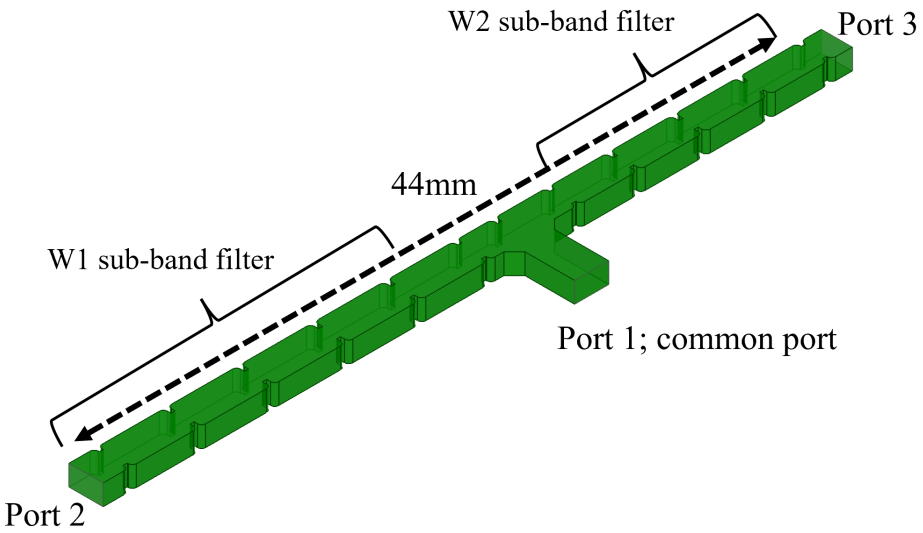

Figure 3.10: TE_{102} mode Diplexer 3D-EM model

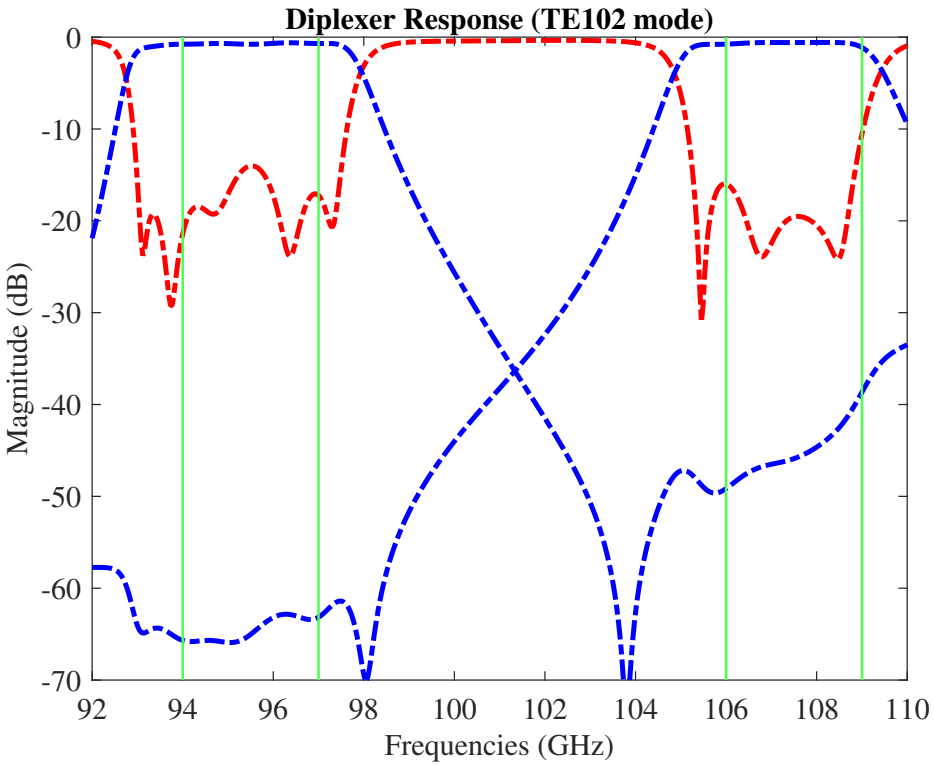

Figure 3.11: Simulated S-parameters for the TE_{102} mode diplexer design

3.3.4 Sensitivity Analysis

In section 2.5, it is already discussed that sensitivity analysis is a crucial step to determine the permissible manufacturing tolerances for a particular design. To determine the design sensitivity, a parametric sweep analysis was conducted on all three Diplexers that were designed and discussed in Section 3.3. The results of this analysis demonstrated that the TE_{102} mode diplexer exhibited significantly higher tolerances, with an allowable range of $\pm 15um$, compared to the TE_{101} mode diplexer, which had a range of $\pm 05um$, and the custom configuration diplexer, which had a range of $\pm 10um$. However, it should be noted that the TE_{102} mode diplexer had a larger overall volume, representing a clear trade-off in achieving lower sensitivity to manufacturing errors. After careful consideration, the research work has concluded that the optimal choice for this study is the **TE_{102} mode diplexer** design.

Table 3.2: Allowable tolerances and size comparison for different configurations

Specifications	**TE101**	**TE102**	**Custom Configuration**
Frequency Range		94-97GHz/106-109GHz	
Size	25.35 x 3.9 mm	44 x 3.9 mm	35 x 3.9 mm
Tolerances	$\pm 05um$	$\pm 15um$	$\pm 10um$

3.3.5 TE_{102} Mode Folded Diplexer Design

As discussed in the introduction chapter, the primary objective of diplexer assembly design is to facilitate FDD configuration in an entire antenna system. To achieve this goal, the diplexer assembly must be integrated with FPA and Beamforming network. Hence, to meet these integration requirements, the overall size of the assembly needs to be reduced by positioning the resonators in a specific folded configuration instead of a straight line as illustrated in 3.12.

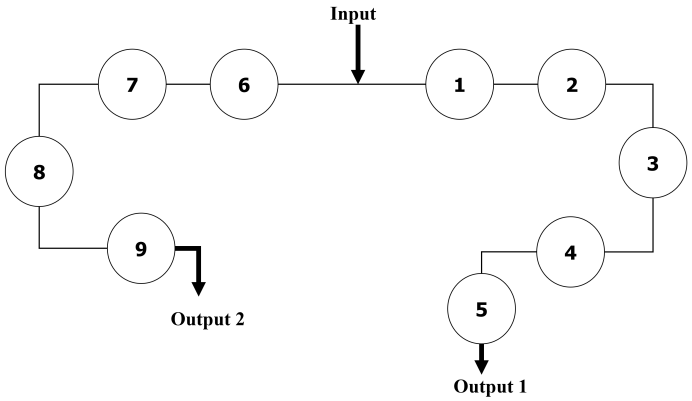

Figure 3.12: Structure of the 09-resonator diplexer in a folded topology

In order to facilitate the CNC milling manufacturing process, the same H-plane T-junction with inductive irises is selected in the folded configuration. The top view of the 9th order folded diplexer structure is shown in Figure 3.13.

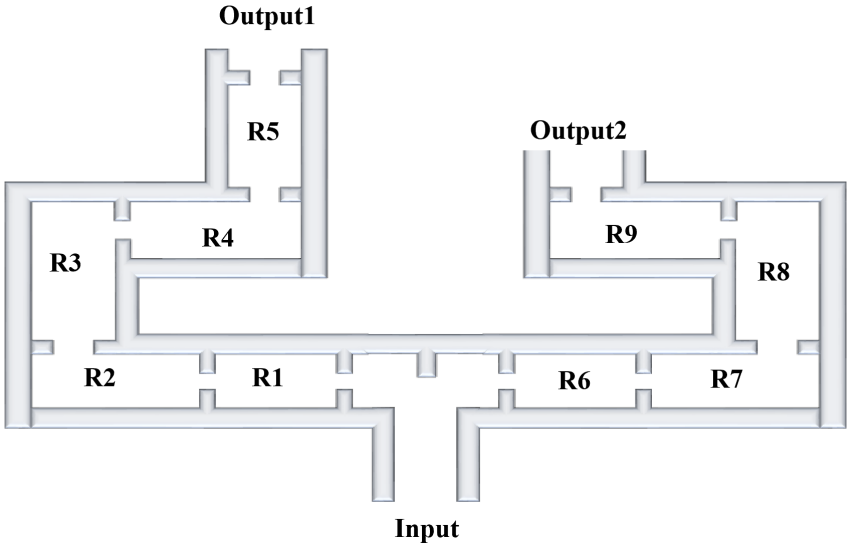

Figure 3.13: Top view of the diplexer architecture. R1 to R9 are the cavity resonators

The most adequate time-saving process in folded diplexer assembly design is to design the folded filters individually and then join them together to form a complete diplexer assembly as a 3D-EM model.

3.3.5.1 TE_{102} mode folded filters

In this section, the three-fold design of TE_{102} mode filters (W1 and W2 sub-bands) is discussed. At first, the resonator cavity lengths and irises widths were set to the dimensions obtained from the coupling matrix method explained in 2.4. The filter was then folded according to the integration specifications as illustrated in Figure 3.13. Subsequently, the filter underwent optimization to achieve performance that was closely aligned with the desired requirements.

It is noteworthy to mention that during the attempt to achieve the desired three-fold configuration for the W2 sub-band filter, difficulties were encountered in optimizing the folding process of the last resonator. Despite the practical feasibility of achieving the desired configuration, it was determined that a more time-efficient approach would be to utilize a five-pole filter instead of a four-pole filter for the W2 sub-band. This adjustment allows for meeting the design requirements while maintaining the overall volume of the diplexer. Consequently, the total number of resonator cavities in the diplexer is increased to ten, with five poles allocated for each filter. Figure 3.14 presents the top view of the modified 10^{th} order folded diplexer configuration.

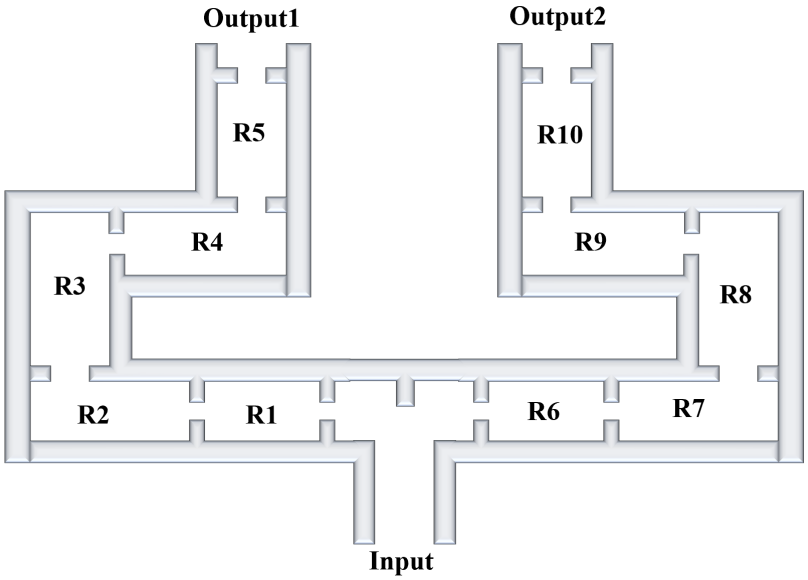

Figure 3.14: Top view of the diplexer architecture. R1 to R10 are the cavity resonators

Five-poles TE_{102} mode W2 sub-band filter The design process begins with the utilization of the Coupling matrix model, as described in Section 2.4, to create an initial straight W2 sub-band filter consisting of five poles. 3D-EM model along with

dimensions and simulated S-parameter results of the filter are displayed in Figure 3.15 and Figure 3.16 respectively. These figures provide a visual representation of the filter's geometry and the corresponding simulated frequency response based on the S-parameters.

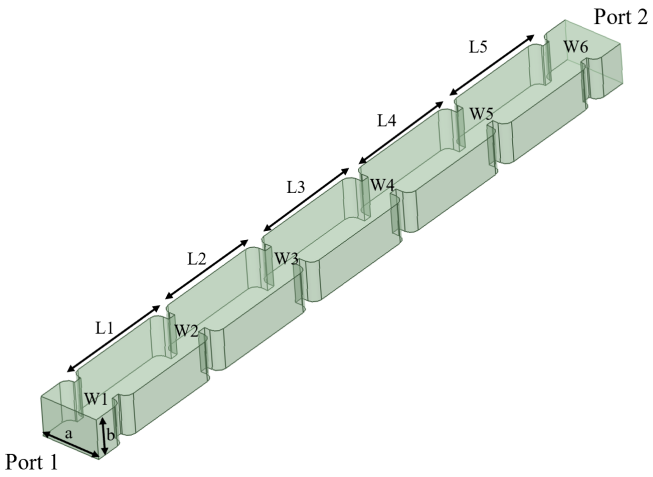

Figure 3.15: Five-poles TE_{102} mode W2 sub-band filter; L1=L5=3.475mm, L2=L4=3.705mm, L3=3.745mm, W1=W6=1.302mm, W2=W5=1.022mm, W3=W4=0.958mm

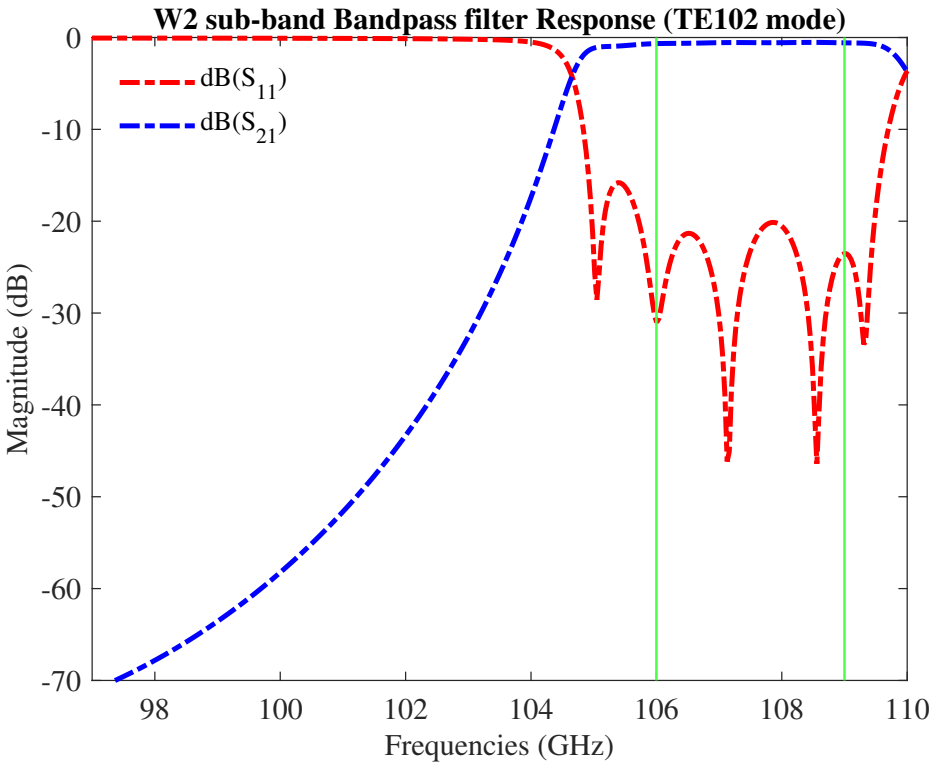

Figure 3.16: Simulated S-parameters for TE_{102} mode W2 sub-band filter (five-poles)

TE_{102} mode W1 and W2 sub-bands folded filters Subsequently, the filters are folded into a targeted three-fold configuration, followed by an optimization process to attain the desired frequency response. The 3D-EM models of the folded filters are depicted in Figure 3.17 and Figure 3.18. These figures illustrate the folded structure of the filters, providing a visual representation of their geometric arrangement after the folding process.

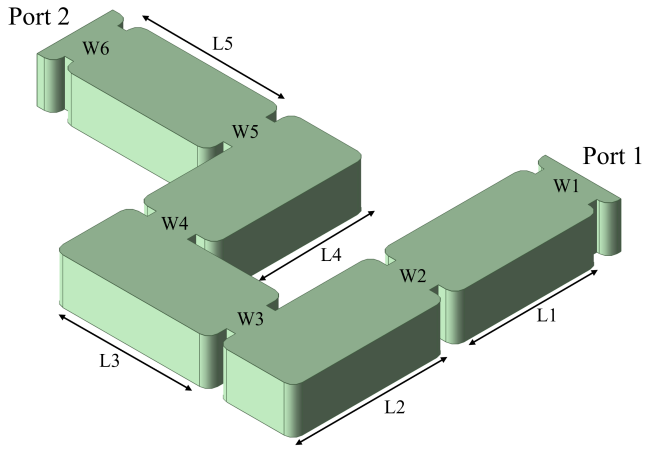

Figure 3.17: Five-poles TE_{102} mode W1 sub-band filter in a folded configuration; L1=L5=4.011mm, L2=L4=4.246mm, L3=4.301mm, W1=W6=1.466mm, W2=W5=1.173mm, W3=W4=1.103mm

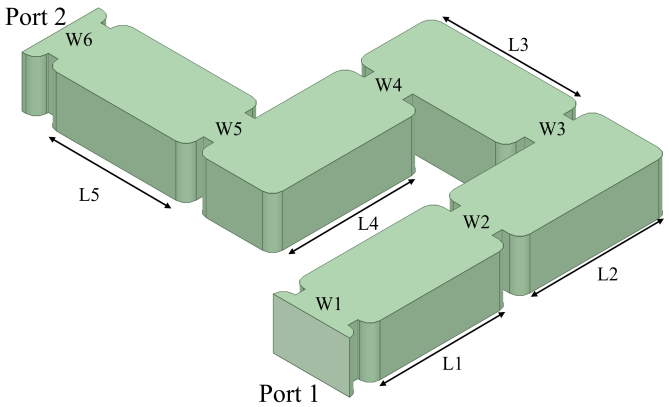

Figure 3.18: Five-poles TE_{102} mode W2 sub-band filter in a folded configuration; L1=L5=3.475mm, L2=L4=3.705mm, L3=3.745mm, W1=W6=1.302mm, W2=W5=1.022mm, W3=W4=0.958mm

3.3.6 Analysis and Assembly of a Compact Diplexer

The subsequent stage involves the integration of the folded filters with the T-junction to form a complete diplexer model. Initially, the EM-circuit co-simulation method is employed to determine the preliminary design dimensions. Subsequently, a comprehensive 3D-EM model is constructed and optimized to achieve the desired frequency

response. This optimized diplexer design is presented in Figure 3.19 and its corresponding simulated performance is illustrated in Figure 3.20

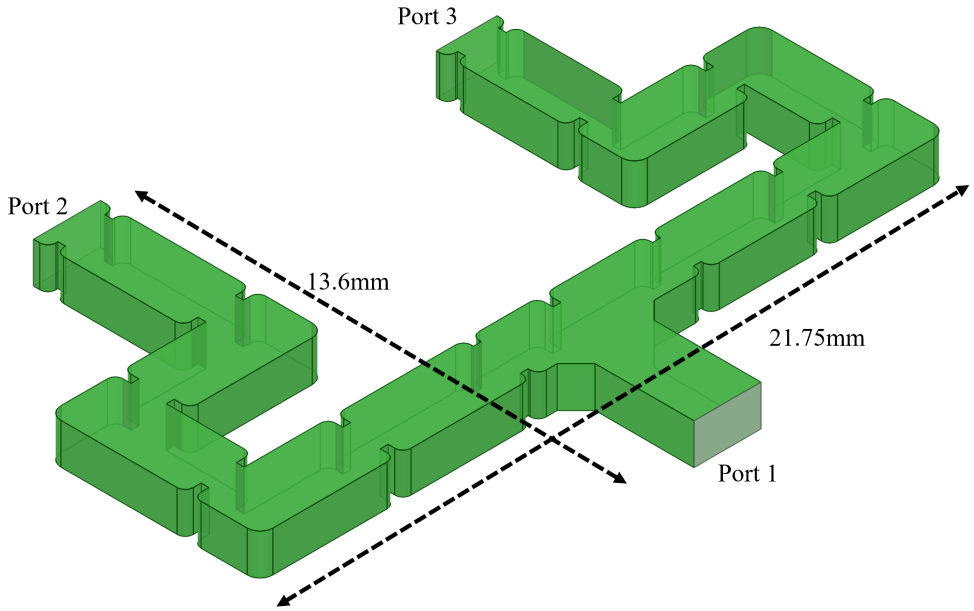

Figure 3.19: TE_{102} mode Diplexer in a folded configuration

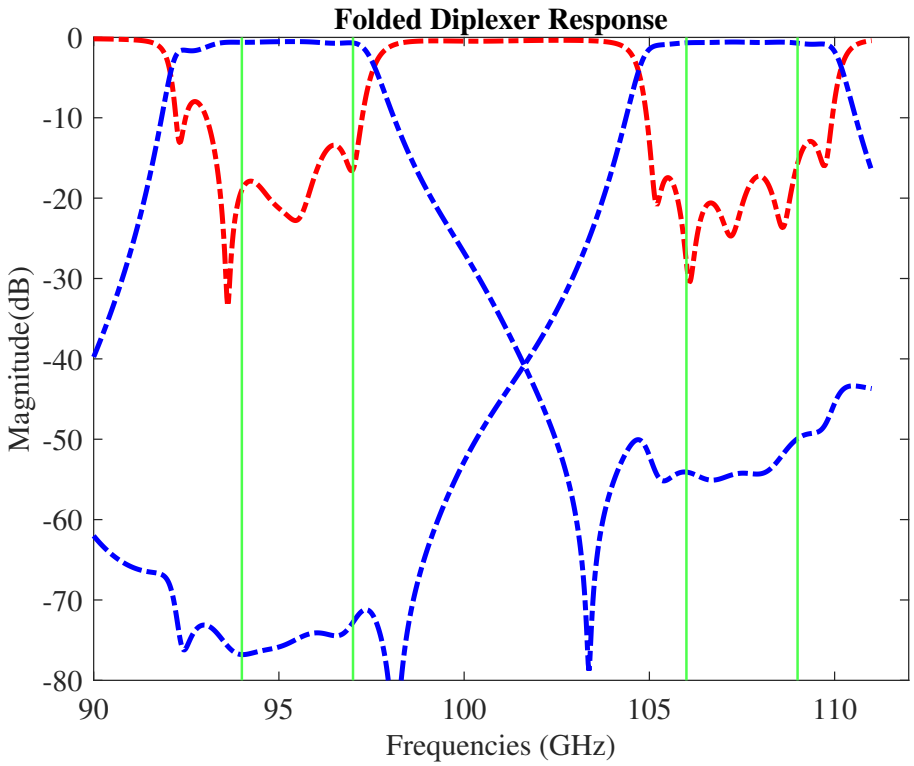

Figure 3.20: Simulated S-parameters for TE_{102} mode Folded Diplexer

Figure 3.21 presents a detailed visual representation of the folded architecture of the diplexer, and highlights its labeled parameters. Table 3.3 complements this

information by presenting the corresponding dimensions of the diplexer. This table offers precise details regarding the specific dimensions of the diplexer's components, enabling valuable insights into its overall configuration and ensuring a thorough understanding of its construction.

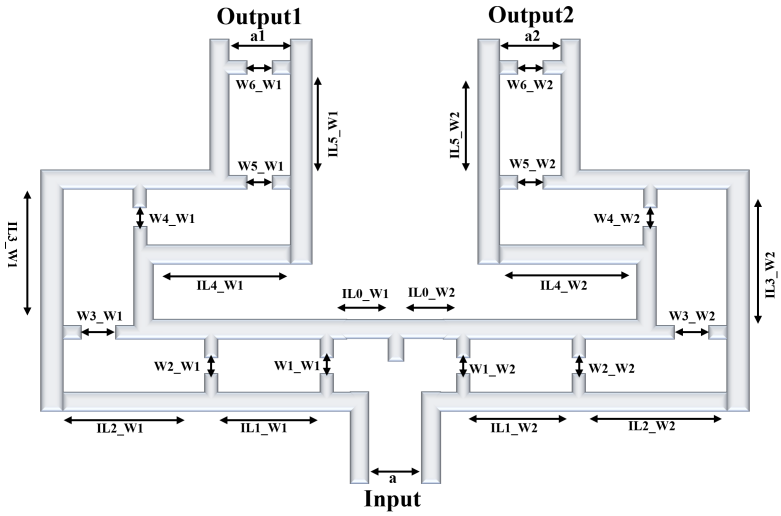

Figure 3.21: Diplexer folded architecture (labeled)

Table 3.3: Diplexer Dimensions

Parameters	Dimensions (mm)	Parameters	Dimensions (mm)
IL1_W1, IL5_W1	4.001	W1_W1, W6_W1	1.466
IL2_W1, IL4_W1	4.236	W2_W1, W5_W1	1.173
IL3_W1	4.30	W3_W1, W3_W1	1.103
IL1_W2, IL5_W2	3.465	W1_W2, W6_W2	1.272
IL2_W2, IL4_W2	3.675	W2_W2, W5_W2	1.032
IL3_W2	3.725	W3_W2, W3_W2	0.958
IL0_W1	2.065	IL0_W2	3.065
a, a1	2.10	a2	1.90

3.4 Design Readiness for manufacturing

The final stages involve specific considerations for the manufacturing preparation of the design. As mentioned earlier in the filter design section, custom waveguide dimensions are employed for the individual filters and the T-junction design. However, to facilitate measurements in the laboratory, standard WR-10 waveguide connectors and terminations are required. Thus, the initial step is to design and incorporate a

waveguide transition from the custom waveguide dimensions to the standard WR-10 dimensions. To enable connectivity for laboratory measurements, the output and input ports need to be connected to standard UG-387/U-M waveguide flanges. These flanges possess specific dimensions and necessitate clearance for seamless connectivity. To fulfill these requirements, waveguide extensions are designed and integrated to expand the output ports of the diplexer assembly. Subsequently, an E-plane step is designed and integrated for all three ports. Initially, all three waveguide ports were positioned in the same plane for simplicity of design. However, for accurate measurements, the pair of output ports and input ports must be oriented 180 degrees opposite in the plane. To address this, an E-plane step is designed, optimized, and incorporated into all three ports, ensuring connectivity to the standard UG-387/U-M waveguide flanges.

Custom waveguide to WR-10 transition

(a) W1 sub-band branch **(b)** W2 sub-band branch

Figure 3.22: Waveguide Transitions for both W1 and W2 sub-bands branches

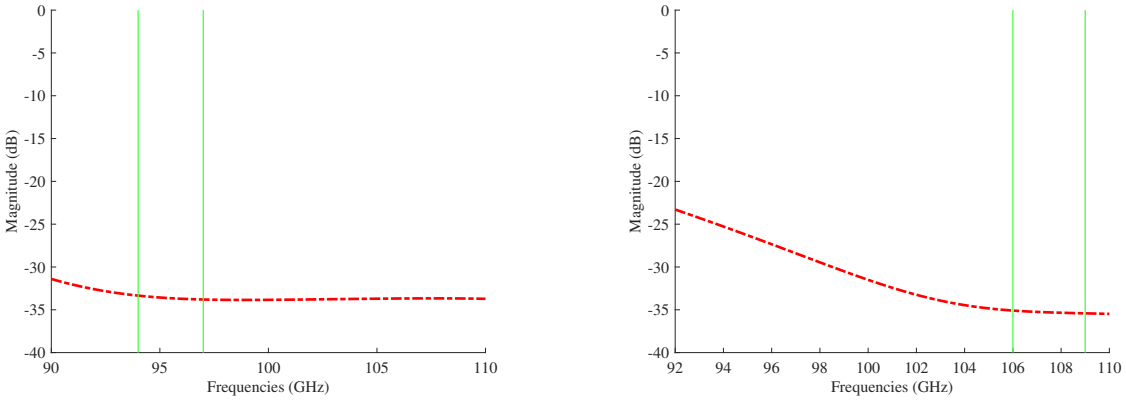

(a) W1 sub-band **(b)** W2 sub-band

Figure 3.23: Simulated S_{11} results for waveguide transitions

Waveguide Extenders

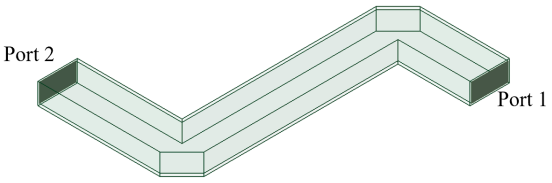

(a) Waveguide extension 3D model

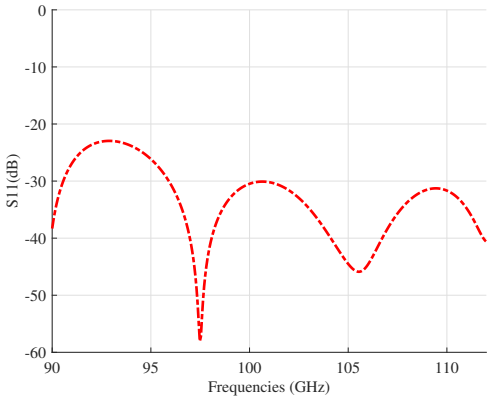

(b) Simulated S_{11} results for WG extension

Figure 3.24: Waveguide extension for fan-out assembly

E-plane step

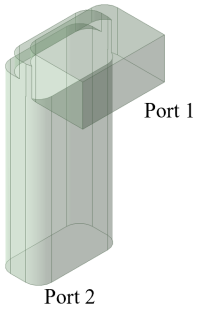

(a) E-plane step 3D-Model

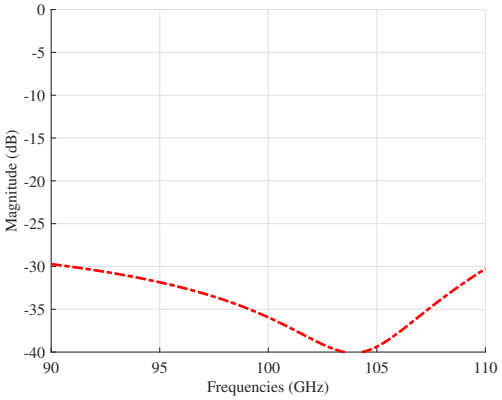

(b) Simulated S_{11} results for E-plane step

Figure 3.25: Waveguide E-plane step for Input/Output ports

Top and Bottom plate design

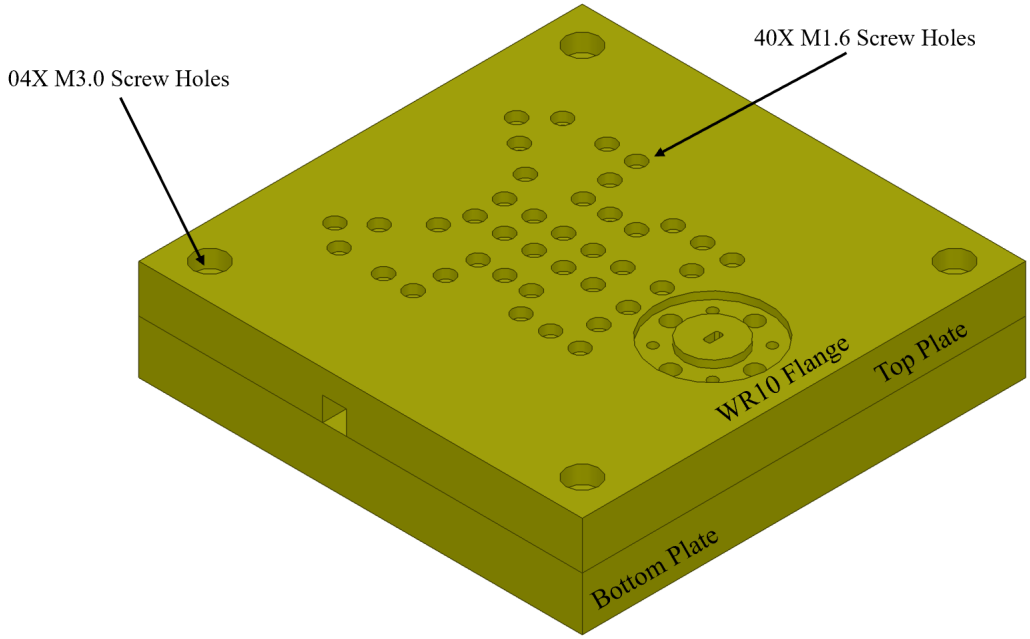

Figure 3.26: Top View of the Final Design Assembly for manufacturing

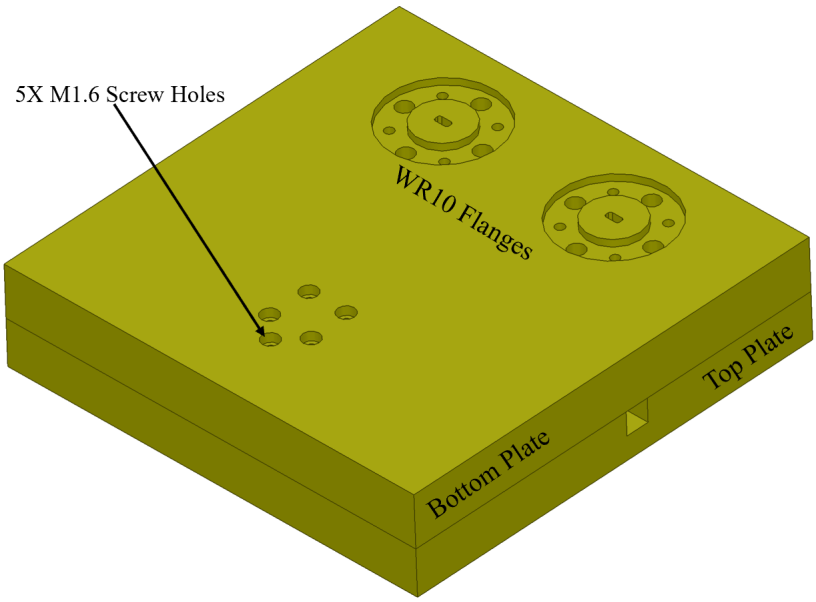

Figure 3.27: Bottom View of the Final Design Assembly for manufacturing

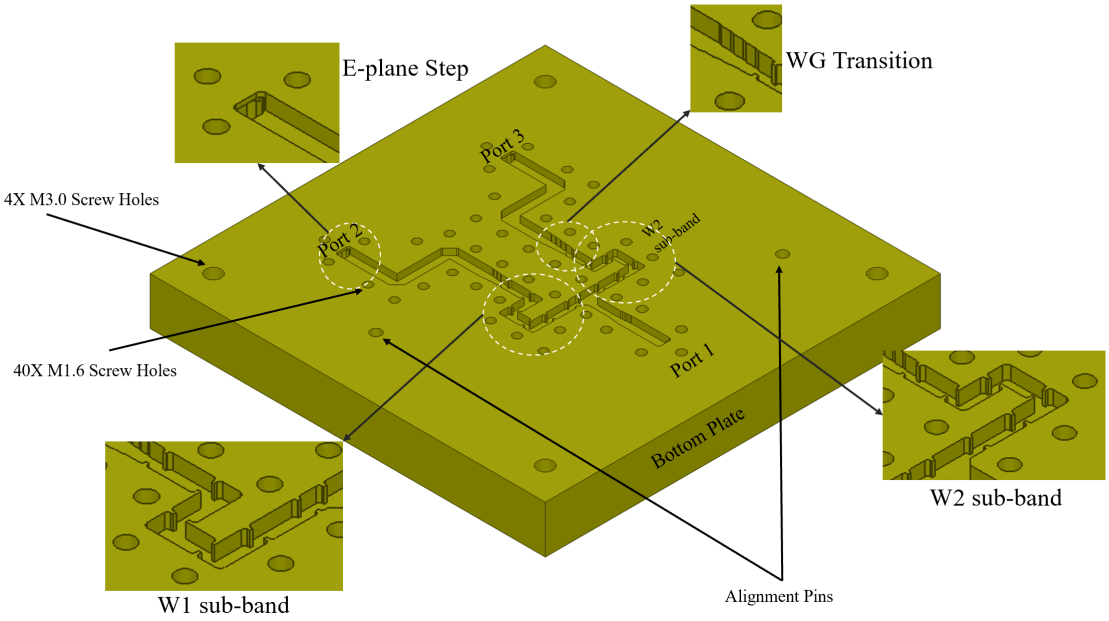

Figure 3.28: Inside View of the Final Design Assembly for manufacturing

3.5 Prototype Measurements and Analysis

To ensure suitability for CNC milling operations, the final design underwent several iterations before reaching the manufacturing stage. Following the completion of these iterations, a prototype diplexer assembly was manufactured, and subsequent measurements were conducted in a laboratory setting. The figures provided below offer a visual representation of the milled diplexer, the complete laboratory setup employed for measurements, and the obtained measurement results. These figures serve to illustrate the physical realization of the diplexer, the experimental environment, and the outcomes of the conducted measurements.

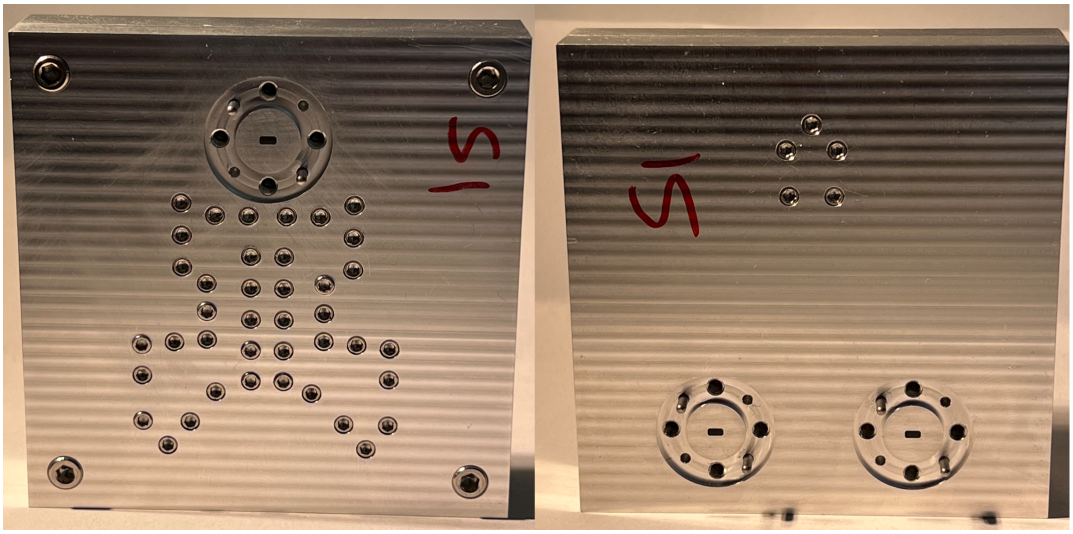

Figure 3.29: Diplexer Assembly manufactured via CNC milling

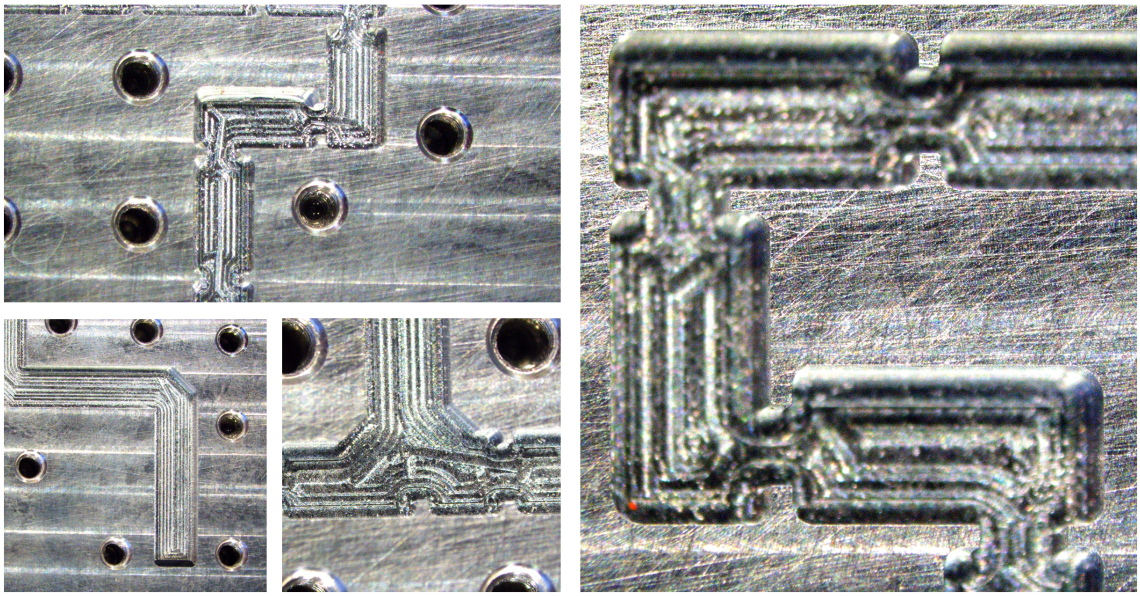

Figure 3.30: Microscopic images of the manufactured diplexer

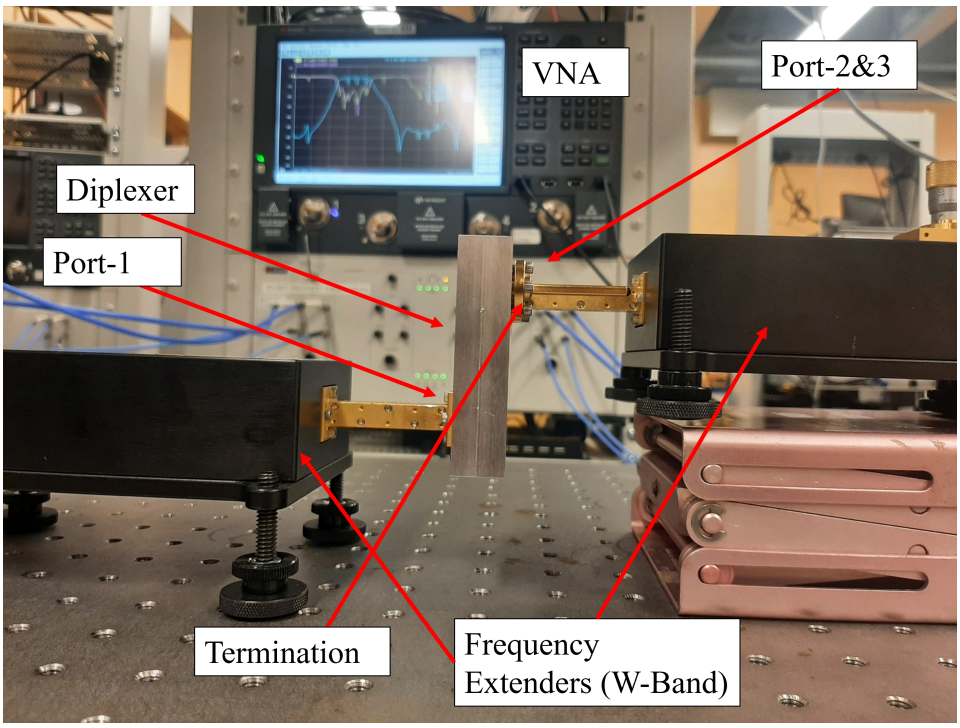

Figure 3.31: Measurement setup for 03-ports measurements of diplexer

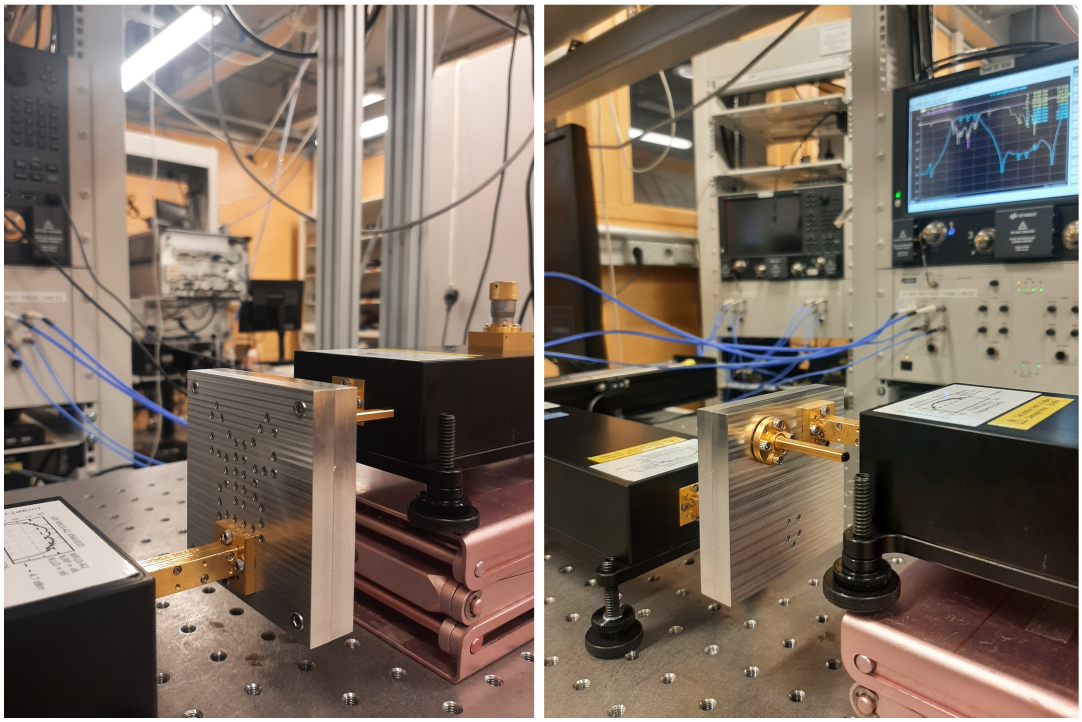

Figure 3.32: Measurement setup (Lateral Views)

Measurements results

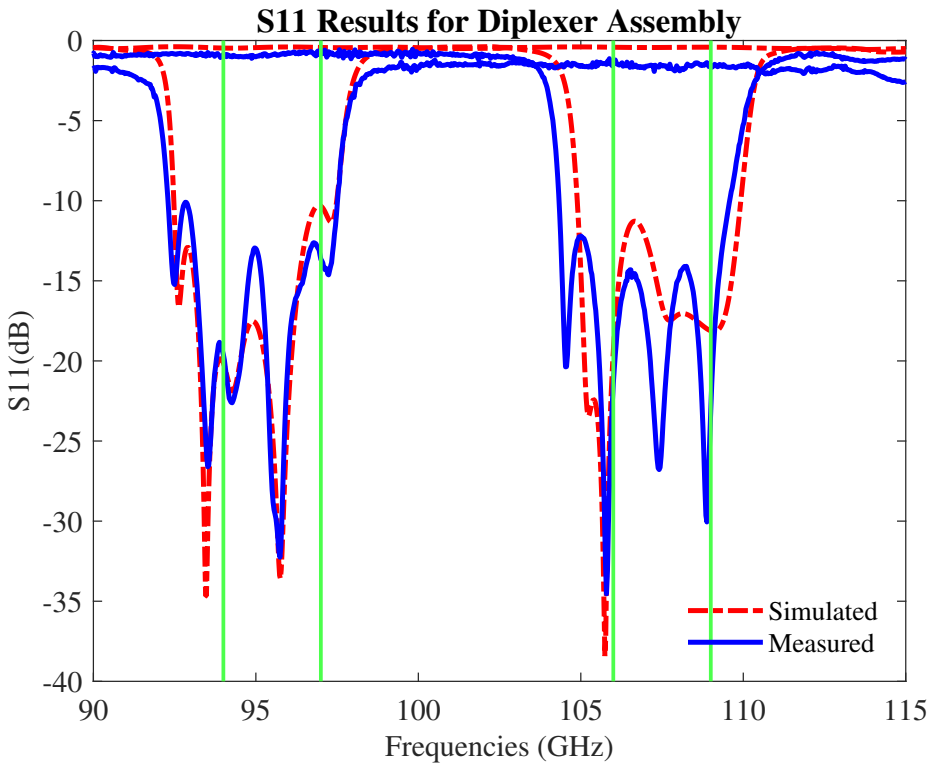

Figure 3.33: S-parameters for diplexer (Measured and Simulated)

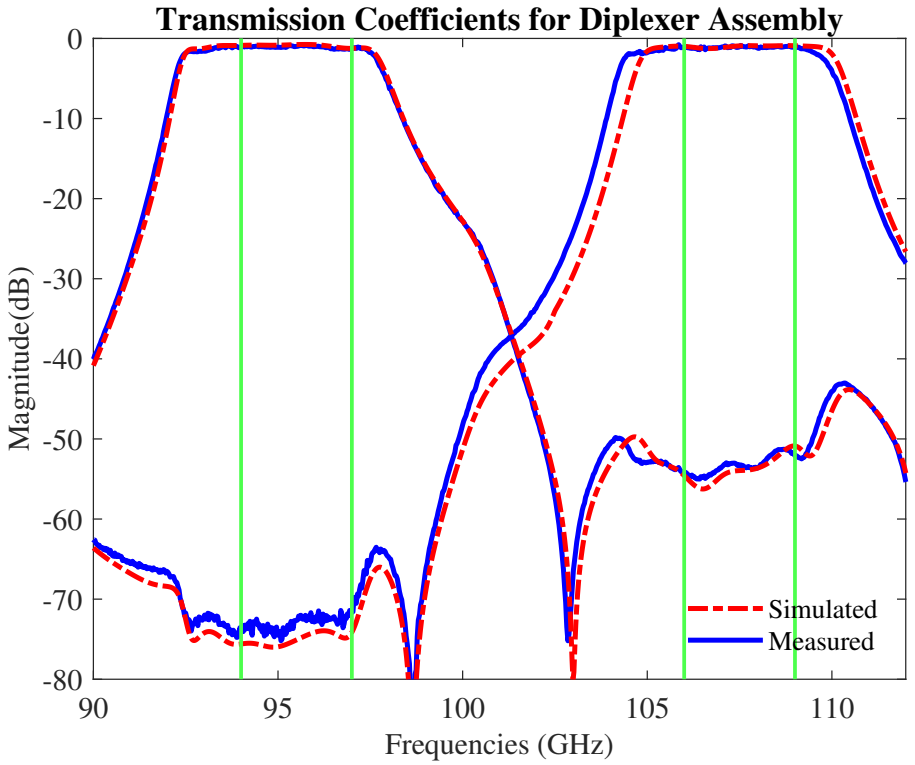

Figure 3.34: S-parameters for diplexer (Measured and Simulated)

The above-presented figures provide clear evidence that the measured results align closely with the simulation results, confirming the successful achievement of the desired performance metrics in the compact diplexer assembly design research project. Although a slight deviation is observed in the W2 sub-band, it does not significantly impact the overall bandwidth coverage for both sub-bands. Thus, the research project demonstrates the successful realization of the diplexer design with the desired frequency response and performance metrics, showcasing the effectiveness of the implemented methodology.

3.6 Literature Comparison

Within the domain of diplexers, a limited number of W-band prototypes manufactured using the precision CNC milling technique have been documented in current literature. Although the available prototypes for direct comparison are scarce, an effort is made to compare the critical discrepancies in measurement results. To this end, Table 3.4 showcases the existing W-band diplexers produced through CNC milling, enabling the observation of competitive outcomes.

Table 3.4: Comparison of W-Band CNC-based Fabricated Diplexers

fc (GHz)	FBW (%)	Insertion Loss (dB)	Return Loss (dB)	Isolation (dB)	Order	Sizes (mm)	References
95.5 / 106.5	11.52 / 10.33	1.5 / 1.7	NA	NA	10	NA	[30]
87.5 / 102.5	5.71 / 4.89	1.0 / 1.0	> 10	25 / 45	06	13.5	[31]
97.5 / 105.5	5.62 / 4.99	0.76 / 0.88	> 21	30 / 40	08	16.14*16.26	[32]
95.5 / 107.5	3.14 / 2.79	1.0 / 1.0	≥ 15	75 / 55	10	21.75*13.6	This work

The results indicate that the compact H-plane diplexer designed in this research work has achieved competitive performance. Notably, the milled diplexer in [32] demonstrates reduced insertion losses and improved reflection coefficient compared to this research work, due to a unique mixed inverter configuration. However, achieving good isolation is a challenge using this configuration, i.e., to attain the desired isolation, a higher-order diplexer is required, which ultimately results in an increased physical size/volume hence this research work has superior performance in terms of isolation with compact size. Additionally, the design is less susceptible to manufacturing tolerances and successfully integrated into an industrial-grade W-band backhaul antenna system.

4

Integration of Modules and Performance Analysis

The ultimate objective of the project is to seamlessly integrate the diplexer assembly consisting of 07 diplexers with the Focal Plane Array (FPA). This chapter focuses on the individual integration of the designed diplexer with the FPA. It also presents a frequency response analysis of the FPA elements integrated with a specific diplexer, offering comprehensive insights. Additionally, the chapter discusses the integration process, along with considerations of miniaturization and optimization

4.1 Integration of diplexer assembly with Focal Plane Array

4.1.1 Focal Plane Array

The innovative and optimized design of the focal plane array (FPA) at 94GHz (Figure 4.2)was carried out by Viktor Chernikov [4]. In [33], an extensive investigation was conducted on various open-ended waveguide antenna elements to determine the most suitable type for the FPA. Among the options explored, the circular open-ended Teflon-filled waveguide (COETW) element was identified as the optimal choice for this research, as depicted in Figure 4.1. The arrangement of the seven elements followed a hexagonal grid pattern as illustrated in the figure.

The design process commenced by carefully selecting an appropriate reflector configuration that aligned with the objectives of minimizing active elements and achieving beam-focusing. To enhance the reflector's aperture efficiency, focal-field analysis [34] was utilized to ascertain the ideal size of the FPA. Consequently, an FPA with a circular aperture diameter of approximately 15 mm (4.7λ) was chosen.

(a) (b)

Figure 4.1: Focal Plane Array designed and optimized for 94GHz:(a)FPA Lateral view (b)Top View [4]

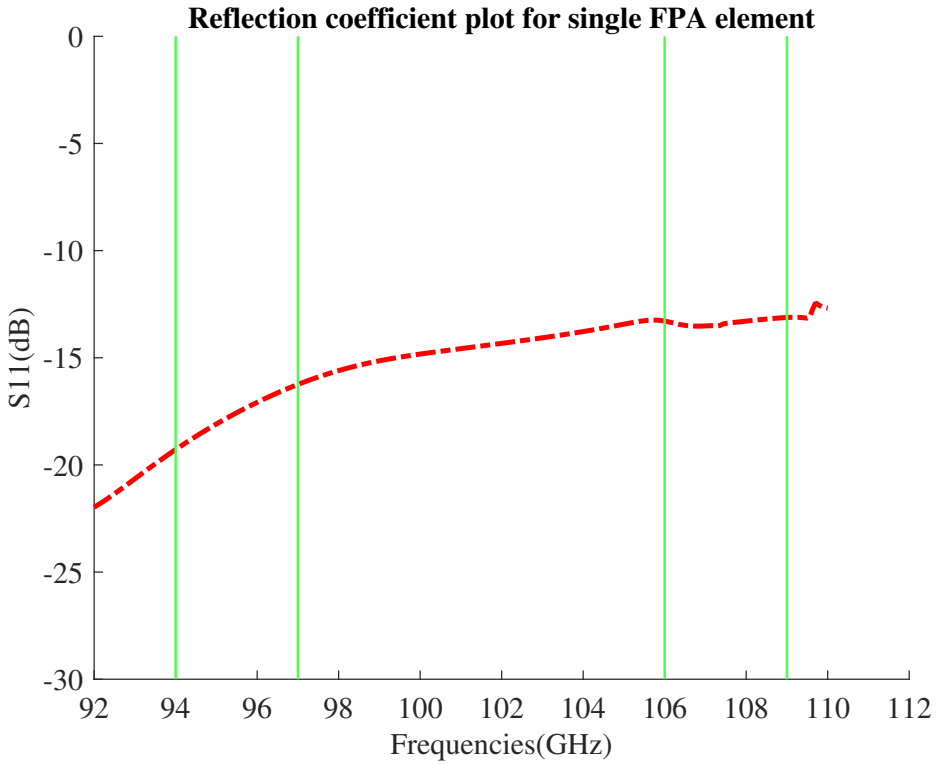

Figure 4.2: Reflection coefficient plot for single FPA element

4.1.2 Integration of Diplexer with Single Antenna Element

To reduce the simulation time and streamline optimization processes, the integration of a single antenna element with a Diplexer is considered. As previously mentioned, the FPA is designed and optimized for the W1 sub-band (94GHz), and adjustments are necessary to ensure optimal operation in both the W1 and W2 sub-bands. Consequently, modifications are made to the FPA and filters (diplexer) to achieve the desired performance. Figure 4.3 illustrates the diplexer integrated with a single element of the Focal plane array. Implementing this approach was aimed to significantly reduce simulation time, simplify the optimization process, and ultimately

achieve the best possible performance because FPA elements are decoupled from each other. The reflection coefficient (S_{11}) at both the output ports of the diplexer is a crucial parameter in optimizing the overall integrated performance and is illustrated in figure 4.4.

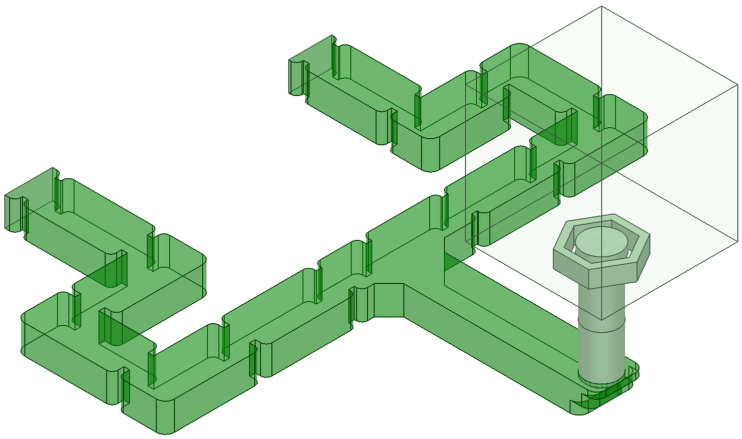

Figure 4.3: Diplexer with a single element of FPA

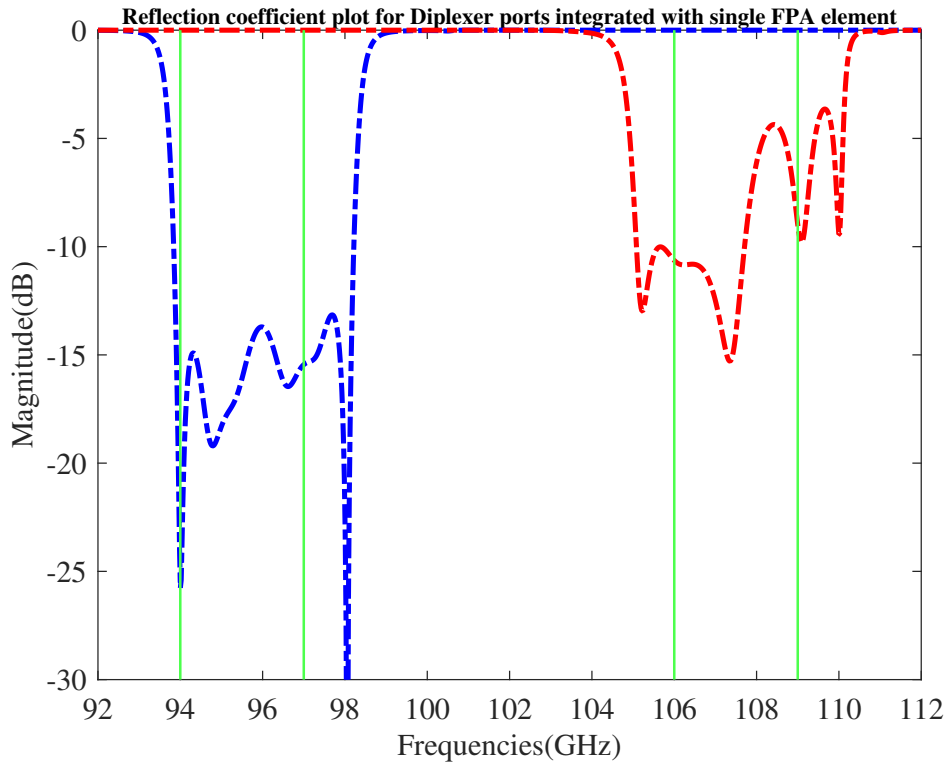

Figure 4.4: Reflection coefficient plot for Diplexer integrated with single FPA element

4.1.3 Integrated Design: Diplexers and Focal Plane Array (FPA)

Once a single diplexer and single antenna element are integrated, the next step involves generating a comprehensive 3D electromagnetic (EM) model of the complete Focal Plane Array (FPA) along with seven diplexers. The elements' integration with diplexers occurs across two distinct layers called top and bottom plates, dictated by the H-plane orientation of the diplexer. The top plate accommodates four diplexers, while the bottom plate houses three diplexers, resulting in seven diplexers. To visually represent the final integration and its dimensions, Figure 4.5 is presented. This figure provides a detailed and intricate arrangement that aims to optimize the performance and functionality of the FPA.

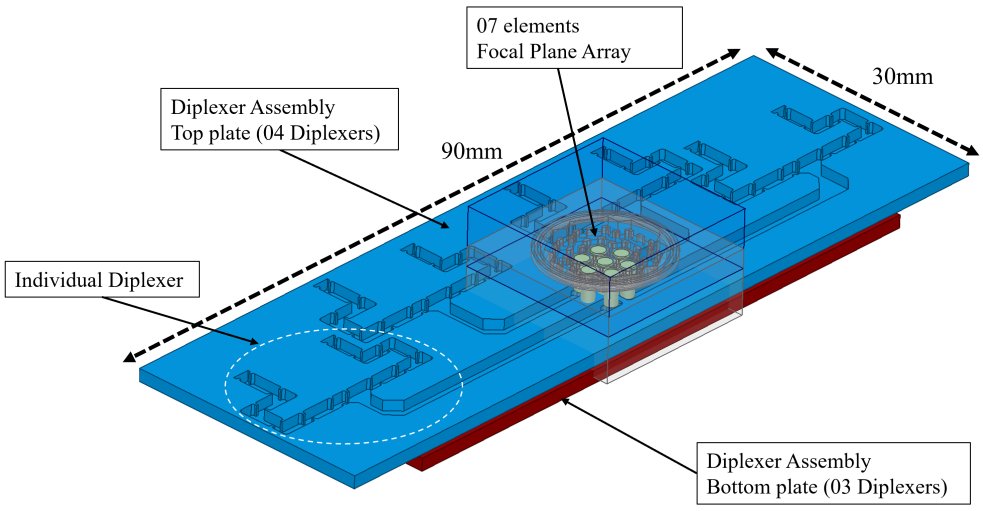

Figure 4.5: FPA with 07 Diplexers integrated

5
Conclusion

This research thesis has successfully presented the design and development of a compact W-band diplexer assembly for Focal Plane Array (FPA) fed reflectors. The primary objective of this research was to design a diplexer assembly that meets stringent requirements for insertion loss, isolation, and frequency selectivity, while also maintaining low sensitivity to manufacturing tolerances and ensuring compactness suitable for integration with FPA-fed reflector systems in wireless backhaul links. The development of this diplexer assembly is of significant importance to the wireless backhaul link proposed in a Vinnova-funded project at Chalmers, which involves electronically steerable antenna systems. This thesis aims to analyze the efficacy of enabling FDD configuration in these steerable antennas.

Throughout this study, we have conducted a comprehensive investigation into the design considerations and challenges associated with the development of a compact W-band diplexer assembly that is less sensitive to manufacturing tolerances. We have analyzed various aspects including the electromagnetic characteristics, impedance matching, isolation, and insertion loss of the diplexer. Multiple design iterations and optimizations were performed to achieve the desired performance parameters, i.e., the reflection coefficient of -15dB or less, insertion loss below -1dB, isolation of 50dB or greater, and allowable tolerance limits for manufacturing errors of $\pm$15um or greater. The diplexer designed in this project was manufactured using precision CNC milling, and extensive measurements were carried out in the laboratory to validate its performance. Furthermore, the diplexer was integrated with the available FPA design, and a 3D EM model was generated to fulfill the integration requirements of this research work. The overall performance of the integrated diplexer and FPA element was found to be highly satisfactory for the desired operations.

Based on our simulations and measurement results, we can confidently conclude that the proposed diplexer assembly successfully meets the specified design goals. It exhibits excellent performance in terms of insertion loss, isolation, and frequency selectivity within the desired W-band frequency range, while also demonstrating low sensitivity to manufacturing tolerances. Moreover, its compact size allows for seamless integration with FPA-fed reflector systems, making it a highly suitable choice for future W-band backhaul applications.

Bibliography

[1] E19(18)09-a1 "radio frequency channel/block arrangements for fixed service systems operating in the bands 92 – 94 ghz, 94.1 – 100 ghz, 102 – 109.5 ghz and 111.8 – 114.25 ghz". Draft, European Communications Committee (ECC).

[2] Chandra M. Kudsia Richard J. Cameron and Raafat R. Mansour. *Microwave Filters for Communication Systems; Fundamentals, Design, and Applications*. John Wiley Sons, Inc., 2018.

[3] John Ross Aitken and Jiasheng Hong. Design of millimetre wave diplexers with relaxed fabrication tolerances. *IET Microwaves, Antennas and Propagation*, 9(8):802–807, June 2015.

[4] Viktor Chernikov, Artem Vilenskiy, Sam Agneessens, Lars Manholm, and Marianna Ivashina. A teflon-filled open-ended circular waveguide focal-plane-array used for sway compensation in w-band 50db-gain backhaul reflector antennas. is submitted for publication in ICEAA, 2023.

[5] Artem R. Vilenskiy, Sohaib Yaqoob Chaudhry, Hsi-Tseng Chou, and Marianna V. Ivashina. Millimeter-wave array antenna architectures employing joint power combining and beam steering for next-generation backhaul applications. In *2023 17th European Conference on Antennas and Propagation (EuCAP)*, pages 1–5, 2023.

[6] Wai-Kai Chen and T. Hong. *Microwave Filters for Communication Systems: Fundamentals, Design, and Applications*. John Wiley & Sons, 2013.

[7] E.M.T Jones George L. Matthaei, Leo Young. *Microwave filter, Impedance Matching Networks and Coupling Structures*. ARTECH House Inc, 1985.

[8] David M. Pozar. *Microwave Engineering*. Wiley, 2011.

[9] Peter Russer and Daniel Sjöberg. *Filters and Filtration Handbook*. Elsevier Science, 5th edition, 2006.

[10] George L. Matthaei, Leo Young, and Edward M. Jones. Microwave filters, impedance-matching networks, and coupling structures. 1980.

[11] O. C. Zienkiewicz and R. L. Taylor. *The Finite Element Method: Its Basis and Fundamentals*. Butterworth-Heinemann, 6th edition, 2005.

[12] Allen Taflove and Susan C. Hagness. *Computational Electrodynamics: The Finite-Difference Time-Domain Method*. Artech House, 3rd edition, 2005.

[13] Roger F. Harrington. *Field Computation by Moment Methods*. Wiley-IEEE Press, 3rd edition, 2001.

[14] R.M. Ano and A.W. Lawson. Microwave filters using quarter wave couplings. Technical Report Technical Report No. 8, NDRC Division 14, Massachusetts Institute of Technology, Research Laboratory of Electronics, June 28 1946.

[15] Seymour B Cohn. Direct-coupled-resonator filters. *Proceedings of the IRE*, 45(2):187–196, 1957.

[16] J.D. Rhodes. A low-pass prototype network for microwave linear phase filters. *IEEE Transactions on Microwave Theory and Techniques*, 18(6):290–301, 1970.

[17] Steve Winder. *Filter Design*. Newnes, illustrated, reprint edition, 1997.

[18] Jia-Sheng Hong and Michael J. Lancaster. *Microstrip Filters for RF/Microwave Applications*. Wiley, 2001.

[19] Hicham Setti, Asmae Mimouni, and Abdelwahed Tribak. Design and manufacturing of iris waveguide filters for satellite communication. *TELKOMNIKA Telecommunication Computing Electronics and Control*, 21(2):247–252, 2023.

[20] R. Levy. Theory of direct-coupled-cavity filters. *IEEE Transactions on Microwave Theory and Techniques*, 15(6):340–348, 1967.

[21] LD Smullin. Design of tunable resonant cavities with constant bandwidth. Technical Report 106, Research Laboratory of Electronics, Massachusetts Institute of Technology, April 1949.

[22] Stephen A. Maas. *Nonlinear Microwave and RF Circuits*. Artech House, 2 edition, 2003.

[23] Giuseppe Setti and Davide Comite. Design of diplexers for microwave communication systems: A review. *International Journal of Microwave and Wireless Technologies*, 9(3):581–591, 2017.

[24] Jiasheng Hong. *Microwave filters and diplexers*. John Wiley & Sons, 2015.

[25] J. Bornemann, J. Uher, and K. Patel. Efficient full-wave cad of waveguide diplexers. In *Proceedings of ANTEM 96 Symposium, Antenna Technology and Applied Electromagnetics*, pages 591–594, 1996.

[26] A. Morini, T. Rozzi, and M. Morelli. New formulae for the initial design in the optimization of t-junction manifold multiplexers. In *1997 IEEE MTT-S International Microwave Symposium Digest*, pages 1025–1028, 1997.

[27] H. Setti, Abdelwahed Tribak, A. Hamichi, JAMAL ZBITOU, and Angel Mediavilla. K-band waveguide t-junction diplexer for satellite communication. *TELKOMNIKA (Telecommunication Computing Electronics and Control)*, 17:549, 04 2019.

[28] Giandomenico Cannone and Matteo Oldoni. High-yield e-band diplexer for fixed radio point-to-point equipment. *International Journal of RF and Microwave Computer-Aided Engineering*, 24, 07 2014.

[29] Wenjie Wu, Daquan Huang, Yaqing Liu, and Chunyong Zhang. Em circuit co-simulation using hfss and ads. In *2017 IEEE International Conference on Computational Electromagnetics (ICCEM)*, pages 107–108. IEEE, 2017.

[30] Cam Nguyen and Kai Chang. Design and performance of a w-band broadband finline diplexer with over 20 ghz bandwidth. In *1985 IEEE MTT-S International Microwave Symposium Digest*, pages 349–352, 1985.

[31] Yi-Chi Shih, Long Q. Bui, and T. Itoh. Millimeter-wave diplexers with printed circuit elements. *IEEE Transactions on Microwave Theory and Techniques*, 33(12):1465–1469, 1985.

[32] C. Bartlett, J. Bornemann, and M. Höft. 3-d-printing and high-precision milling of w-band filter components with admittance inverter sequences. *IEEE Transac-*

tions on Components, Packaging and Manufacturing Technology, 11(12):2140–2147, December 2021.

[33] V. S. Chernikov, A. R. Vilenskiy, and M. V. Ivashina. Design considerations for focal-plane array antennas for 6g millimeter-wave backhaul links. In *Proc. of the 2023 IEEE International Symposium on Antennas and Propagation and USNC-URSI Radio Science Meeting - AP-S/URSI*, 2023.

[34] M. V. Ivashina, M. N. M. Kehn, and P. S. Kildal. Optimal number of elements and element spacing of wide-band focal plane arrays for a new generation radio telescope. In *The Second European Conference on Antennas and Propagation, EuCAP*, Edinburgh, 2007.

A

Appendix 1

In this appendix, we aim to emphasize key areas of future work and provide recommendations based on the findings of this research study. While the development of a compact W-band diplexer assembly for FPA-fed reflectors has been accomplished, there exist several avenues for further exploration that can enhance its performance, functionality, and effectiveness in future backhaul applications. The following are recommended areas for future work:

Advanced and Low-cost Manufacturing Techniques: For future recommendations, it is advised to further explore and implement advanced and low-cost manufacturing techniques, such as additive manufacturing, microfabrication, and 3D printing, to effectively reduce the size and weight of the diplexer assembly while ensuring its performance remains uncompromised. These techniques have the potential to revolutionize the manufacturing process by enabling precise fabrication of intricate structures and optimizing space utilization within the assembly. Additionally, the utilization of new and innovative materials, such as metamaterials or plasmonic structures, may also be investigated to enhance the miniaturization process even further. By successfully integrating advanced manufacturing techniques and novel materials, there is the potential to achieve significant advancements in the miniaturization of the diplexer assembly. This not only contributes to the field of research but also offers potential cost benefits in the manufacturing process for mass production.

Thermal Management: The examination of thermal effects and the development of effective thermal management techniques for the diplexer assembly is also a critical aspect. The antenna system proposed in this project operates within the W-band frequency range at high power levels, making efficient heat dissipation paramount. Failure to address thermal management adequately may result in performance deterioration or even damage to the components. Considering the operating conditions of the W-band antenna system, it is imperative to implement robust strategies to mitigate thermal issues. This involves employing efficient heat dissipation methods, optimizing material selection for heat conduction and insulation, and implementing appropriate cooling mechanisms. By diligently addressing the thermal challenges, we can ensure the preservation of optimal performance and longevity of the components, thus guaranteeing the reliability and stability of the overall antenna system.

Bandwidth Enhancement: This study primarily focuses on narrow-band filters designed for specific sub-bands within the complete W-band frequency range. The

diplexer assembly developed in this research covers a bandwidth of 6GHz, with each sub-band spanning 3GHz. However, it should be noted that the complete W-band is characterized by its wideband nature. Therefore, it would be worthwhile to investigate methods that can enhance the bandwidth of the diplexer assembly without sacrificing its compactness. One potential avenue for exploration involves delving into novel filter designs, such as frequency-selective surfaces or multi-layered structures. These innovative approaches have the potential to achieve broader frequency coverage, thereby expanding the bandwidth of the diplexer assembly. By incorporating such advanced techniques, it is possible to maintain the desired compact form factor of the diplexer while simultaneously accommodating the wide bandwidth requirements of the complete W-band.

Integration with complete Antenna system: Integration with the complete antenna system warrants further investigation, specifically in terms of the diplexer assembly's integration with the beamforming network. It is essential to study the impact of the diplexer on the overall system performance, which encompasses crucial factors such as radiation pattern, gain, and beamforming capabilities. Conducting a comprehensive analysis of the diplexer's integration with the complete antenna system allows for a deeper understanding of its influence on system-level performance. Thus, by addressing the integration aspects, researchers can maximize the overall performance and functionality of the backhaul antenna systems, ultimately leading to enhanced operational capabilities and improved system efficiency.

Reliability and Environmental Considerations: Reliability and environmental considerations play a crucial role in assessing the diplexer assembly's performance and ensuring its suitability for real-world deployment. To achieve this, it is imperative to conduct thorough and extensive reliability testing, specifically evaluating the diplexer assembly's behavior and performance under diverse environmental conditions. Factors such as temperature variations, humidity, and vibration should be carefully examined to validate the robustness and resilience of the assembly. This can ensure that the diplexer assembly can operate consistently and effectively, meeting the demands and challenges imposed by different environmental scenarios encountered in practical deployments.

By diligently addressing these aforementioned recommendations, there exists an opportunity to drive further advancements in the field of compact W-band diplexers implementation for FPA-fed reflectors. This concerted effort will result in tangible improvements in performance metrics, expanded functionality, and enhanced applicability within next-generation W-band backhaul systems. The implementation of these recommendations will serve as a catalyst for pushing the boundaries of diplexer technology, ensuring its alignment with the evolving demands and requirements of modern communication systems. Ultimately, this endeavor will contribute to the overall progress and success of W-band backhaul systems, empowering the seamless and efficient transmission of data in the rapidly advancing telecommunications landscape.

DEPARTMENT OF ELECTRICAL ENGINEERING
CHALMERS UNIVERSITY OF TECHNOLOGY
Gothenburg, Sweden
www.chalmers.se

CHALMERS
UNIVERSITY OF TECHNOLOGY